




Cite this: *Nanoscale Horiz.*, 2024, 9, 1262

Recent progress in atomically precise metal nanoclusters for photocatalytic application

Yuanxin Du,* Chengqi Li, Yali Dai, Haijiao Yin and Manzhou Zhu *

Photocatalysis is a widely recognized green and sustainable technology that can harness inexhaustible solar energy to carry out chemical reactions, offering the opportunity to mitigate environmental issues and the energy crisis. Photocatalysts with wide spectral response and rapid charge transfer capability are crucial for highly efficient photocatalytic activity. Atomically precise metal nanoclusters (NCs), an emerging atomic-level material, have attracted great interests owing to their ultrasmall size, unique atomic stacking, abundant surface active sites, and quantum confinement effect. In particular, the molecule-like discrete electronic energy level endows them with small-band-gap semiconductor behavior, which allows for photoexcitation in order to generate electrons and holes to participate in the photoredox reaction. In addition, metal NCs exhibit strong light-harvesting ability in the wide spectral UV–near IR region, and the diversity of optical absorption properties can be precisely regulated by the composition and structure. These merits make metal NCs ideal candidates for photocatalysis. In this review, the recent advances in atomically-precise metal NCs for photocatalytic application are summarized, including photocatalytic water splitting, CO₂ reduction, organic transformation, photoelectrocatalytic reactions, N₂ fixation and H₂O₂ production. In addition, the strategy for promoting photostability, charge transfer and separation efficiency of metal NCs is highlighted. Finally, a perspective on the challenges and opportunities for NCs-based photocatalysts is provided.

Received 8th May 2024,
Accepted 21st June 2024

DOI: 10.1039/d4nh00197d

rsc.li/nanoscale-horizons

1. Introduction

Nanocatalyst research has been flourishing over the past few decades. With the improvement of catalysts' controllable synthesis methods and fine characterization analysis techniques,¹ the current nanocatalyst family can be classified into relatively large sized nanoparticles (NPs), mid-sized nanoclusters (NCs) with a size less than 2 nm, and ultrasmall single-atom catalysts (SACs). The study of NPs, the starting point of nanocatalysis, reveals the contribution of the low coordination environment and quantum size effect on the metal surface to the ultra-high catalytic activity. However, just as nanochemists have been disturbed by the fact that no two NPs are identical, the polydispersity of NPs (*i.e.* the heterogeneity in size, morphology, and surface environment) makes it difficult to achieve tailored catalytic performance based on the structure–activity relationship. Metal NCs are composed of few to a few hundred metal atoms and bridge the gap between NPs and SACs. With the advantages of the ultrasmall size, abundant surface

unsaturated coordinative sites, unique atomic stacking mode, and quantum confinement effect, metal NCs have received great attention in catalysis. Unlike the continuous energy band in NPs and single atomic orbital in SACs, metal NCs exhibit a discrete energy level and behave like molecules, and some larger ones even span nonmetallic-to-metallic regimes. Especially, in such a small size range, the quantum confinement effect becomes much more significant, and even one atom change will bring about a huge change in the catalytic activity. In addition, metal NCs with a precise composition, structure, and surface environment provide the opportunity to investigate in depth the catalytic mechanism and build the catalyst structure–property relationship.^{2–5} A clear structure and high atom utilization are also the advantages of SACs;⁶ however, there is no single atom in the true sense because a single atom cannot exist without a support. Besides, it is difficult to simultaneously activate multiple reactants by SACs to achieve high activity in a complex reaction. Recently, some studies have reported that few-atom catalysts show superior activity than SACs in certain reactions.

In terms of photocatalysis, the ideal catalyst needs to have strong light-harvesting ability, can effectively generate photo-induced electrons and holes, and rapidly transfer and separate charge carriers.^{7–9} Due to the surface plasmon resonance (SPR) effect induced by the collective oscillations of electrons on the

Department of Materials Science and Engineering, Centre for Atomic Engineering of Advanced Materials, Key Laboratory of Structure and Functional Regulation of Hybrid Materials of Ministry of Education, Key Laboratory of Functional Inorganic Material Chemistry of Anhui Province, Anhui University, Hefei 230601, China.
E-mail: duyuanxin@ahu.edu.cn, zmz@ahu.edu.cn

surface of the metal NPs, conventional Au and Ag NPs exhibit unique size or morphology-dependent optical absorbance property. However, the optical absorption range is usually limited to the visible light region, for example, the typical SPR absorption peak of Au and Ag NPs is in the range of 520–570 nm and 450–500 nm, respectively. Unlike the narrow visible light absorption of plasmonic metal NPs, metal NCs exhibits wide light absorption range from the UV to the near IR region. Moreover, the absorption property of metal NCs is various and diverse, which can be precisely regulated by the composition and structure.^{10,11} On the other hand, the ultrasmall size endows metal NCs with discrete electronic energy level-like molecular behavior different from the metal-like behavior of large metal NPs.¹² Metal NPs themselves cannot be excited to generate electrons and holes and usually act as the co-catalyst to improve the photocatalytic activity. For example, the Schottky junction is formed at the interface when metal NPs contact with the semiconductor, and it can build an effective one-way electron transfer channel for facilitating the photogenerated charge transfer and separation. However, metal NCs with the highest occupied molecular orbital (HOMO) and the lowest occupied molecular orbital (LUMO) gap can serve as a small-band-gap semiconductor and exhibit the capability of generating electrons and holes under light excitation.^{13–15} Theoretically, metal NCs themselves can be used as the photocatalyst or it can be combined with another semiconductor to construct a hetero-junction photocatalyst. Therefore, metal NCs with the merits of strong light response and semiconductor-like characteristic show great application potentials in photocatalysis (Scheme 1).

The application of metal NCs in catalysis has developed rapidly and is in a state of explosion in recent years; however, the application in photocatalysis is still lagging behind the development of electrocatalysis, thermal catalysis, liquid phase catalysis, and so on.^{11,16–20} The ultrasmall size is a

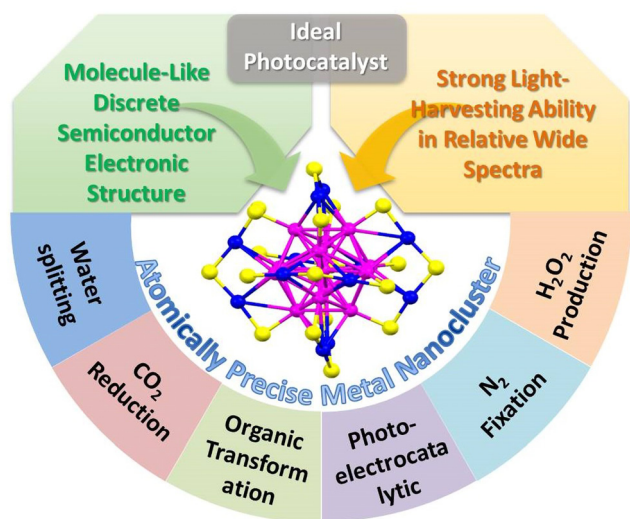
double-edged sword, although it contributes to the abundant catalytic active sites and unique electronic structure; it causes high surface energy, leading to the unfavorable agglomeration of metal NCs during the photocatalytic reaction. In addition to the poor photostability, the ultrasmall size makes charge carrier recombination easy, resulting in a short carrier lifetime. Recently, various synthesis strategies have been developed to construct NCs-porous support composites to avoid the aggregation of NCs and provide a synergic effect for enhanced catalysis; especially, NCs encapsulated in metal organic frameworks (MOFs) is a classical and effective method for improved catalytic stability and activity.^{21–23} Inspired by these NCs-based composites works, many researches propose a strategy of coupling with the other material to fabricate the NCs-based heterostructure to improve the photostability and prolong the carrier lifetime of NCs in order to overcome the inherent defects.

This review includes the recent progress of atomically-precise metal NCs in photocatalytic water splitting, CO₂ reduction, organic transformation, photoelectrocatalytic reaction, and other reactions such as N₂ fixation and H₂O₂ production over the last five years (Scheme 1). The strategy of constructing the NCs-based heterostructure with improved photostability and charge transfer and separation efficiency is summarized and highlighted. In addition, the current challenges and future opportunities faced by NCs-based photocatalysts are provided.

2. Photocatalytic applications of NCs

2.1 Photocatalytic water-splitting

With the proposal of the carbon emission reduction plan and the deepening of the green economy plan, hydrogen energy has become the focus of the world's attention. Due to the low density, high calorific value, and zero-pollution during combustion, hydrogen is called the “ideal energy source” in the 21st century. With the development of fuel cells and new energy vehicles, hydrogen energy is expected to replace fossil energy and officially enter the world energy stage. Photocatalytic water splitting technology can use ready-made solar energy to produce hydrogen from water and has been considered as a clean and environment-friendly hydrogen production method.^{24–29} Generally, photocatalytic water splitting includes three main steps: firstly, the formation of photogenerated electron-hole pairs, secondly, the separation and migration of the generated electron and hole, finally, the participation in water splitting to produce H₂ and O₂. From the aspect of thermodynamics, the energy position of the conduction band (CB) and valence band (VB) of the photocatalyst is required to be more negative and positive than that of H⁺/H₂ (0 V vs. NHE) and O₂/H₂O (1.23 V vs. NHE) for photocatalytic H₂ and O₂ evolution, respectively.^{2,25} In 2013, Negishi *et al.* loaded glutathione-protected Au₂₅(GSH)₁₈-(GSH = Glutathione) NCs on BaLa₄Ti₄O₁₅ as co-catalysts, which increased the photocatalytic water splitting activity by 2.6 times.³⁰ Since then, atomically precise metal NCs have been widely applied to photocatalytic water splitting. Here, only the related researches in the last 5 years are summarized.



Scheme 1 The merits and applications of atomically-precise metal NCs as ideal candidates for photocatalysis.

Pt NCs-based photocatalyst

Due to the excellent photogenerated carrier separation ability, Pt-based materials have been regarded as one of the best co-catalysts. However, the high cost limits the wide application. Pt NCs with small size and high mass activity attract great attention. Lu *et al.* synthesized $\text{Pt}_5(\text{GSH})_{10}$ NCs and immobilized them on multi-armed CdS nanorods (NRs).³¹ The presence of Pt-S₄ active sites were confirmed by X-ray absorption fine structure (XAFS) spectroscopy. Based on the results of ultrafast transient absorption (TA) spectroscopy, Pt NCs could extract the photoinduced electrons of CdS NRs, leading to effective charge separation. Therefore, the Pt_5 -CdS composite exhibited an improved photocatalytic H_2 production activity of $13.0 \text{ mmol h}^{-1} \text{ g}^{-1}$ (under 300 W xenon lamp irradiation with $\lambda > 420 \text{ nm}$), 5.9 times higher than that of CdS NRs.

The ultrasmall size of NCs endows not only high activity but also poor stability. The porous material can act as a support to confine the NCs, preventing their growth or aggregation. Huang *et al.* utilized MIL-125-NH₂ as a support to encapsulate Pt NCs based on the *in situ* auto-reduction method.³² Firstly, the amino groups of MIL-125-NH₂ reacted with HCHO to form MIL-125-CH₂OH with reduction ability. Secondly, MIL-125-CH₂OH was immersed in Pt salt precursor solution. Finally, the Pt NCs were obtained by *in situ* auto-reduction without any additional reducing agent (Fig. 1(a)). The obtained Pt NCs were uniformly dispersed in the cavities of MIL-125-CH₂OH with the size of 1–2 nm. With the optimal Pt NCs amount, the Pt(1.5)/MIL-125-NH-CH₂OH showed the highest photocatalytic H_2 production rate of $4496.4 \text{ } \mu\text{mol g}^{-1} \text{ h}^{-1}$ under $\lambda > 420 \text{ nm}$ visible light irradiation in the mixture of CH₃CN and H₂O system with triethanolamine (TEOA) as the sacrificial agent. Due to the high reactive property of the amino groups, it is speculated that other metal NCs-based composites can be

synthesized through the *in situ* auto-reduction method for other applications.

Similar to MOFs, covalent organic frameworks (COFs) are another kind of porous functional support consisting of various ligands connected by covalent bonds. Due to the adjustability of the structure, it provides the opportunity to rationally design and control the deposition of metal NCs. Li *et al.* synthesized a novel COF named PY-DHBD-COF with an adjacent hydroxyl group and imine bond in each constitutional unit (Fig. 1(b)–(e)).³³ The periodically distributed –OH and imine-N sites created an adsorption environment for Pt species. Under light irradiation, the adsorbed Pt ions were *in situ* reduced to Pt NCs by photo-generated electrons. The optimized Pt NCs-COF with 1 wt% Pt NCs loading exhibited a high photocatalytic H_2 generation activity of $42\,432 \text{ } \mu\text{mol g}^{-1} \text{ h}^{-1}$ (under $\lambda > 420 \text{ nm}$ visible light irradiation in H₂O with ascorbic acid as the sacrificial agent) due to the exposed large active surface.

Au NCs-based photocatalyst. Wang *et al.* fabricated $\text{Au}_{25}(\text{L-Cys})_{18}$ NCs (L-Cys = L-cysteine)/graphitic carbon nitride (g-C₃N₄) heterostructure *via* a facile wet-impregnation method.³⁴ The intimate interface contact and the appropriate energy band structures facilitate efficient photogenerated charge separation, leading to an increase in the photocatalytic H_2 evolution activity. Under the conditions of visible light irradiation and addition of triethanolamine as the sacrificial agent for holes, the optimized $\text{Au}_{25}(\text{L-Cys})_{18}$ NCs/g-C₃N₄ showed an H_2 production rate of $320 \text{ } \mu\text{mol h}^{-1} \text{ g}^{-1}$ (under $\lambda > 420 \text{ nm}$ visible light irradiation in aqueous solution with TEOA as the sacrificial agent), which was 1.7 and 3 times higher than that of photo-reduced Au/g-C₃N₄ and Pt/g-C₃N₄, respectively. In addition, $\text{Au}_{25}(\text{L-Cys})_{18}$ NCs/g-C₃N₄ displayed favorable stability during three cycles with only a 15% decrease in the H_2 production rate, while the photoreduced Au/g-C₃N₄ exhibited a 40.5% decrease.

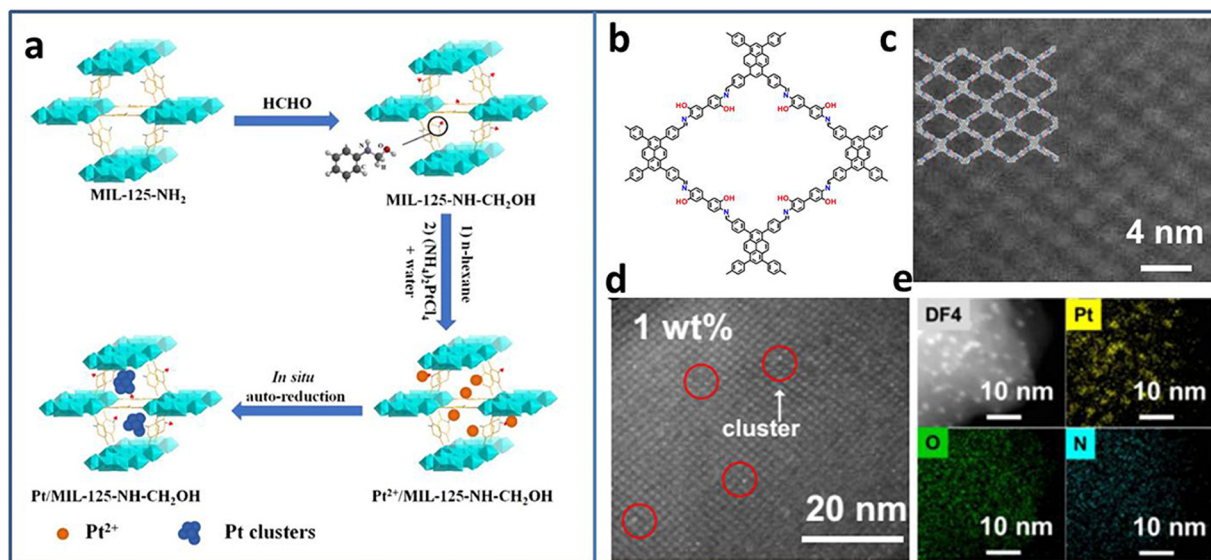


Fig. 1 (a) Steps for the synthesis of Pt/MIL-125-NH-CH₂OH. (b) The structure and (c) the high-angle annular dark-field scanning transmission electron microscopy (HAADF-STEM) image of PY-DHBD-COF. (d) HAADF-STEM image and (e) EDX mapping of 1 wt% Pt-loaded PY-DHBD-COF. Reproduced with permission from ref. 32,33, copyright Springer Nature.

Metal NCs can serve as a photosensitizer to enhance the photocatalytic activity; however, sometimes the poor stability limits their application. Dai *et al.* reported that metal NCs could spontaneously transform to metal NPs under light irradiation, which may result in reduced photoredox activity.³⁵ Fu *et al.* compensated the photosensitization loss of metal NCs by judiciously utilizing self-transformed metal NPs as interfacial Schottky-type charge mediators to build unidirectional charge flow for enhancing the charge transfer efficiency.³⁶ The CdS@CdTe@PDDA@Au_x (PDDA = poly(diallyldimethylammonium chloride)) multilayered core-shell heterostructure was fabricated in the following three steps: first, partial transformation of CdS nanowires (NWs) to ultrathin CdTe layer, then the modification of the PDDA interim layer to convert the surface charge state, and finally, the electrostatic self-assembly of Au_x@GSH (Fig. 2(a)). The electron-trapping ability of the PDDA layer and Schottky-type unidirectional electron flow of self-transformed metal NPs form a long-range cascade charge transfer chain to synergistically accelerate the electron separation on CdS@CdTe; therefore, the photocatalytic H₂ generation activity under the visible light irradiation of CdS@CdTe@PDDA@Au_x was enhanced.

Due to the high surface energy caused by the ultrasmall size of NCs, the easy aggregation induced by the light irradiation results in the catalytic activity loss. Coupling with a photoactive support with a porous structure can not only solve the problem of poor stability of NCs but also improves the catalytic activity by the synergy effect. Yao *et al.* stabilized Au₂₅(L-Cys)₁₈ NCs on photoactive porous UiO-66-NH₂ by the formation of amide covalent bond (Fig. 2(b)).³⁷ Due to the strong metal-support interaction, the obtained UiO-66-NH₂-Au₂₅(L-Cys)₁₈ exhibited enhanced photostability and photocatalytic activity for H₂ production, compared to the mixed UiO-66-NH₂/Au₂₅(PET)₁₈ (PET = 2-phenylethanethiolate). A series of thermodynamic and kinetic experiments revealed that UiO-66-NH₂-Au₂₅(L-Cys)₁₈ possessed lower reaction energy barrier, faster charge carrier generation and transfer efficiency, which was the underlying reason for the improved photocatalytic activity.

In the NCs-based heterostructure, the presence of ligands at the interface usually prevents the contact between the reactant and NCs, leading to a decrease in the catalytic activity. Calcination can remove some ligands. However, over calcination will lead to NCs aggregation and loss of the specific size-related

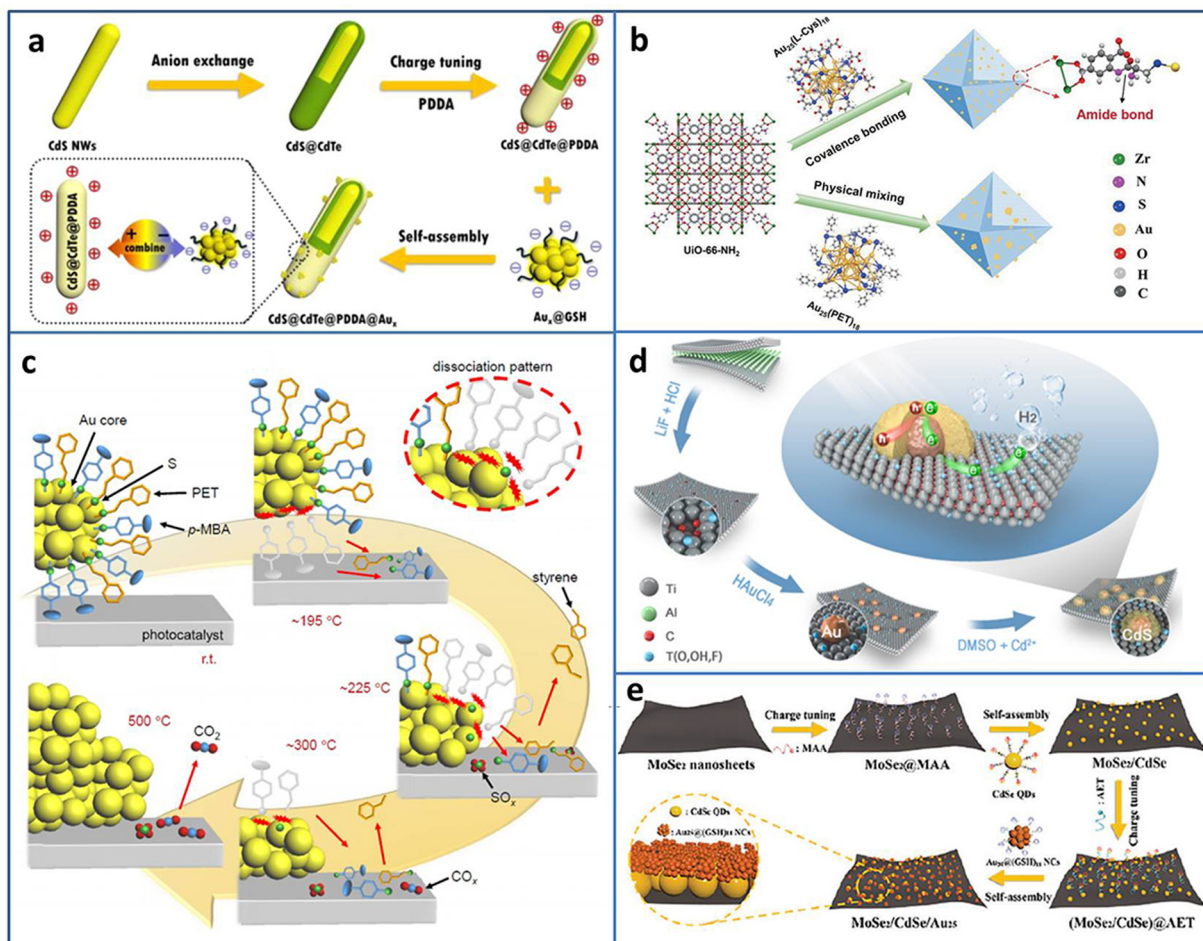


Fig. 2 (a) Construction of CdS@CdTe@PDDA@Au_x. (b) Covalent binding Au₂₅(L-Cys)₁₈ NCs and UiO-66-NH₂. (c) Ligand desorption process during the calcination of Au₂₅(PET, p-MBA)₁₈/BaLa₄Ti₄O₁₅. (d) Preparation of CdS@Au/MXene. (e) Fabrication of MoSe₂/CdSe QDs/Au₂₅ NCs. Reproduced with permission from ref. 36–40, copyright American Chemical Society, Springer Nature, and Wiley-VCH GmbH.

activity of NCs. Kawawaki *et al.* explored the influence of calcination on the ligand removal process and the size change of NCs by taking the metal-oxide-supported 2-phenylethane-thiolate protected Au₂₅ NCs as the examples.³⁸ Ligand desorption with the increase in temperature takes place in three steps: (1) the ligand dissociation on the NCs surface; (2) the generated compounds adsorption on the support; (3) the compounds desorption from the support (Fig. 2(c)). By controlling the calcination process, a water-splitting photocatalyst based on NCs with high activity and stability was created.

Constructing metal NCs-based heterostructure is an effective way to promote carriers separation and improve the photocatalytic activity. In addition to the well-known wide-band-gap TiO₂, some novel semiconductors with excellent photocatalytic activity have emerged in recent years. Li *et al.* utilized reductive Ti vacancy in Ti_{3-x}C₂T_y MXene to *in situ* construct core-shell CdS@Au (Fig. 2(d)).³⁹ The ternary CdS@Au/MXene exhibited two Schottky barriers at the interface, and the charge transferred from CdS to Au NCs and Au NCs to MXene. With the optimal Au NCs and MXene contents, the CdS@Au/MXene showed 5371 $\mu\text{mol g}^{-1} \text{h}^{-1}$ H₂ production rate, 26.6 times higher than that of CdS. Yan *et al.* fabricated MoSe₂/CdSe quantum dots (QDs)/Au₂₅(GSH)₁₈ NCs Z-scheme heterostructure by cascade electrostatic self-assembly method (Fig. 2(e)).⁴⁰ The possible photocatalytic H₂ production pathway of MoSe₂/CdSe QDs/Au₂₅ NCs was followed was: CdSe QDs and Au₂₅ NCs could generate photoinduced e⁻ and h⁺, and an Z-scheme charge transfer was formed between CdSe QDs and Au₂₅ NCs. Due to the metal-like property, MoSe₂ served as a terminal

electron acceptor to accelerate charge separation. The electron trapped by MoSe₂ participated in the reduction of H⁺/H₂O to H₂.

Ag NCs-based photocatalyst. Liang *et al.* also utilized electrostatic self-assembly strategy to elaborately couple Ag_x NCs (Ag₃₁(GSH)₁₉, Ag₁₆(GSH)₉, and Ag₉(GSH)₆) with CdS and Zn_{0.5}Cd_{0.5}S with the help of the surface-charged ligand of NCs.⁴¹ Based on the suitable energy level alignment, Ag_x NCs produced photo-induced electrons and holes under light irradiation, which flow to the CB and VB of transition metal chalcogenides (TMCs), respectively, presenting the typical type II charge transport pathway, which is beneficial to prolong the carrier lifetime and promote charge migration (Fig. 3(a)). The Ag_x NCs/TMCs heterostructure shows significantly enhanced photoactivities toward the anaerobic selective photoreduction of nitroaromatics to amino derivatives and photocatalytic H₂ evolution.

Besides acting as a photosensitizer to expand the light absorption region, metal NCs can be treated as a small-band-gap semiconductor to build a heterojunction. Wang *et al.* modified TiO₂ with Ag₄₄(SR)₃₀ (SR = thiolate) NCs to study the charge transfer behavior at the interface.⁴² Changing the excitation light region from visible to full solar spectrum, the type-II charge transport pathway was constructed between TiO₂ and Ag₄₄ NCs, and thus 3 orders of magnitude increase in the photocatalytic H₂ production rate ($\sim 7.4 \text{ mmol h}^{-1} \text{ g}_{\text{catalyst}}^{-1}$) was obtained (Fig. 3(b)). By the analysis of ultrafast TA spectroscopy, the role of Ag₄₄ NCs was assigned to the light-absorber and small-band-gap semiconductor co-catalyst under UV/Vis

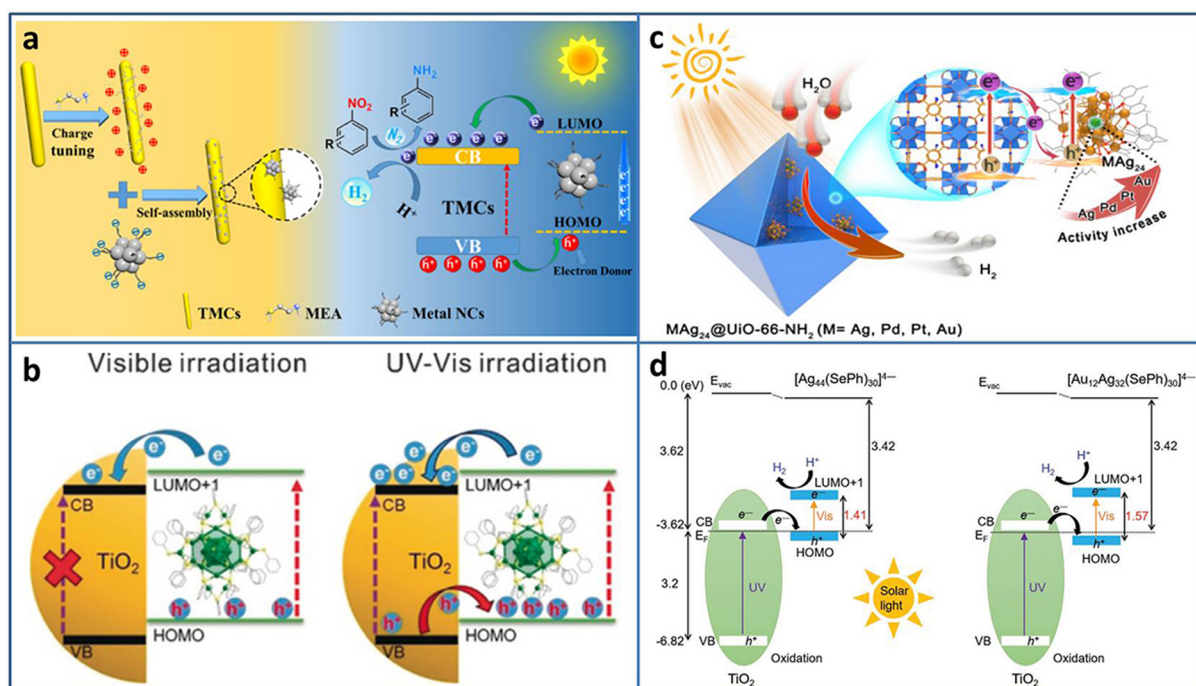


Fig. 3 (a) Construction and photocatalytic mechanism of Ag_x NCs (Ag₃₁, Ag₁₆, Ag₉)/TMC composites. (b) The excitation comparison of TiO₂-Ag₄₄ NCs under visible/UV-vis light irradiation. (c) Illustration of M₁Ag₂₄@UIO-66-NH₂ (M = Ag, Pd, Pt, and Au) for photocatalytic H₂ production. (d) Energy level diagram of Ag₄₄/TiO₂ and Au₁₂Ag₃₂/TiO₂. Reproduced with permission from ref. 41–44; copyright American Chemical Society and Wiley-VCH GmbH.

light irradiation. The enhanced light response and charge transfer both contributed to the enhanced photocatalytic activity of the Ag₄₄-TiO₂ composite.

Constructing an effective charge transfer channel and driving force is helpful to enhance the photocatalytic activity. Zhu *et al.* fabricated Pt₁Ag₂₈-BTT/CoP (BTT = 1,3,5-benzenetrithiol) NCs-based heterostructure through the Co-S interface.⁴⁵ Due to the strong built-in electric field and Co-S interfacial charge transfer channel, Pt₁Ag₂₈-BTT/CoP shows an obvious improvement in photocatalytic H₂ production with 24.89 mmol·h⁻¹·g⁻¹ H₂ production rate, which is 1.49, 2.29, and 5.21 times higher than that of Pt₁Ag₂₈-BDT/CoP (BDT = 1,3-benzenedithiol), Ag₂₉-BDT/CoP, and CoP. In Pt₁Ag₂₈-BTT, central Pt atom doping makes the band alignment between NC and CoP, and the surface S modification provides the opportunity to construct an effective interface charge transport channel, both contributing to the enhanced photocatalytic performance. In addition, the stable and intimate interface connection benefits in the long-term photostability of the NCs-based heterostructure; Pt₁Ag₂₈-BTT/CoP shows almost unchanged catalytic activity during five consecutive recycling tests.

To avoid metal NCs from aggregation, Jiang *et al.* encapsulated M₁Ag₂₄ (M = Ag, Pd, Pt, Au) NCs with 2,4-dimethylbenzenethiolate as the ligand into UiO-66-NH₂ based on the electrostatic interaction.⁴³ Compared to Ag NPs@UiO-66-NH₂, Ag₂₅ NCs@UiO-66-NH₂ displayed 5.6 times enhancement in the photocatalytic H₂ production rate (under $\lambda > 380$ nm light irradiation in the mixture of CH₃CN and H₂O system with TEOA as the sacrificial agent). The influence of the central heteroatom type on the photocatalytic activity was also investigated; the activity order was Au₁Ag₂₄ NCs@UiO-66-NH₂ > Pt₁Ag₂₄ NCs@UiO-66-NH₂ > Pd₁Ag₂₄ NCs@UiO-66-NH₂ > Ag₂₅ NCs@UiO-66-NH₂ (Fig. 3(c)). Femtosecond time-resolved TA spectroscopy demonstrated that the order of charge carrier lifetime of the composite was consistent with that of the photocatalytic activity. X-ray photoelectron spectroscopy (XPS) under the conditions of dark and light irradiation revealed the formation of Z-scheme charge transfer between M₁Ag₂₄ NCs and UiO-66-NH₂.

Thanks to the development of the synthesis with atomic-level control, the opportunity of investigation of the core-shell nanomaterial structure-property relationship is given. Boot-haraju *et al.* synthesized selenolated Au₁₂Ag₃₂ NCs consisting of an Au icosahedron core and Ag dodecahedron shell by the galvanic exchange method.⁴⁴ Compared to the homometal analog Ag₄₄ NCs, Au₁₂Ag₃₂ NCs exhibited near-infrared-II photoluminescence (PL) and enhanced stability. Based on the interaction with the oxygen vacancy of TiO₂, Au₁₂Ag₃₂ NCs were immobilized on TiO₂. Owing to the favorable energy structure of the Au₁₂Ag₃₂ NCs that aligns well with TiO₂ for enhanced photogenerated carrier separation, Au₁₂Ag₃₂/TiO₂ showed significant enhancement in photocatalytic H₂ evolution (6810 $\mu\text{mol g}^{-1} \text{h}^{-1}$), about 6.2 times higher than that of Ag₄₄/TiO₂ (Fig. 3(d)).

Non-noble metal NCs-based photocatalyst. Compared to Au and Ag NCs that have been well studied in recent years, the development of other non-noble metal NCs is in the primary

stage. Cao *et al.* synthesized 20-core copper(I)-alkynyl NCs (UJN-Cu₂₀) by the one-pot solvothermal method.⁴⁶ Due to the protection of ethinyloestradiol ligand, the surface of UJN-Cu₂₀ was exposed with abundant hydroxyl groups (Fig. 4(a)). With the help of hydrogen bonding interactions, UJN-Cu₂₀ was further anchored onto the surface of TiO₂ nanosheets (NSs) (Fig. 4(b)). The surface hydroxyl was confirmed to be useful for the uniform immobilization of NCs compared to Cu₁₄@TiO₂-NSs without hydrogen-bonding interactions. The obtained UJN-Cu₂₀-TiO₂ exhibited higher H₂ production activity (13 mmol g⁻¹ h⁻¹) than bare TiO₂ NSs (0.4 mmol g⁻¹ h⁻¹) under 300 W xenon lamp irradiation. Due to the appropriate energy levels, the UJN-Cu₂₀-TiO₂ heterostructure follows Z-scheme photogenerated carrier transport (Fig. 4(c)), which was evidenced by the hydroxyl radical capture test. The superior photoactivity for H₂ evolution was attributed to good proton affinity, enhanced light absorption, and faster charge separation.

Tian *et al.* utilized double-crown Ni₆(SCH₂Ph)₁₂ NCs protected by benzyl thiol ligands as the co-catalyst and deposited it on TiO₂ by the solvent evaporation method for enhanced photocatalytic H₂ evolution (Fig. 4(d)).⁴⁷ In the mixture of methanol and water system, Ni₆/TiO₂ showed an H₂ production rate of 5600 $\mu\text{mol g}_{\text{cat}}^{-1} \text{h}^{-1}$, turnover frequency (TOF) of 2800 s⁻¹, and apparent quantum efficiency (AQE) of 7.8% at 365 nm excitation. TA spectroscopy was conducted to investigate the electron migration between Ni₆ NCs and TiO₂, and the results demonstrated that the photogenerated electron injection was from TiO₂ to Ni₆ NCs, which was consistent with the XPS and superoxide and hydroxyl radicals trapping results. In addition, the benzyl group may be the photogenerated electron-hole recombination center, which was important for the enhancement in the photocatalytic activity, confirmed by calcination removing ligands and phenethyl or butyl group replacement experiments.

Metal chalcogenide NCs, such as supertetrahedral T_n, P_n, and C_n NCs, can be regarded as the smallest QDs and considered as promising photosensitizers. Wang *et al.* synthesized supertetrahedral T₄ NCs of [Cd₃In₁₇Se₃₁]⁵⁻ with excellent solubility ($\geq 100 \text{ mg mL}^{-1}$ in dimethyl sulfoxide).⁴⁸ T₄ NCs not only played the role of a visible light absorber but also served as a charge separator. The T₄ NCs/TiO₂ showed a remarkable improvement in the photocatalytic H₂ production of 328.2 $\mu\text{mol g}^{-1} \text{h}^{-1}$ in aqueous solution with TEOA as the sacrificial agent, compared to TiO₂ (~ 0) and T₄ NCs (19.5 $\mu\text{mol g}^{-1} \text{h}^{-1}$) (Fig. 4(e)). In addition, T₄ NCs/TiO₂ exhibited high stability with almost no change in the 50 h photocatalytic H₂ production test. Wu *et al.* fabricated a series of T₄-Cd_{4-x}Zn_x/g-C₃N₄ (x = 0, 1, 2, 3, 4) heterostructures (Fig. 4(f)).⁴⁹ By tuning Zn doping content, the optimized T₄-Cd₁Zn₃/g-C₃N₄ with a suitable band structure showed the highest photocatalytic H₂ production rate of 288 $\mu\text{mol g}^{-1} \text{h}^{-1}$ in aqueous solution with TEOA as the sacrificial agent due to the enhanced interfacial charge transfer. Zhang *et al.* decorated [Mo₂S₁₂]²⁻ NCs on TiO₂ through a facile impregnation method.⁵⁰ The intimate contact between [Mo₂S₁₂]²⁻ NCs and TiO₂ effectively promoted the charge transfer and the abundant bridging S in the [Mo₂S₁₂]²⁻ NCs served as active sites; thereby, the [Mo₂S₁₂]²⁻ NCs/TiO₂

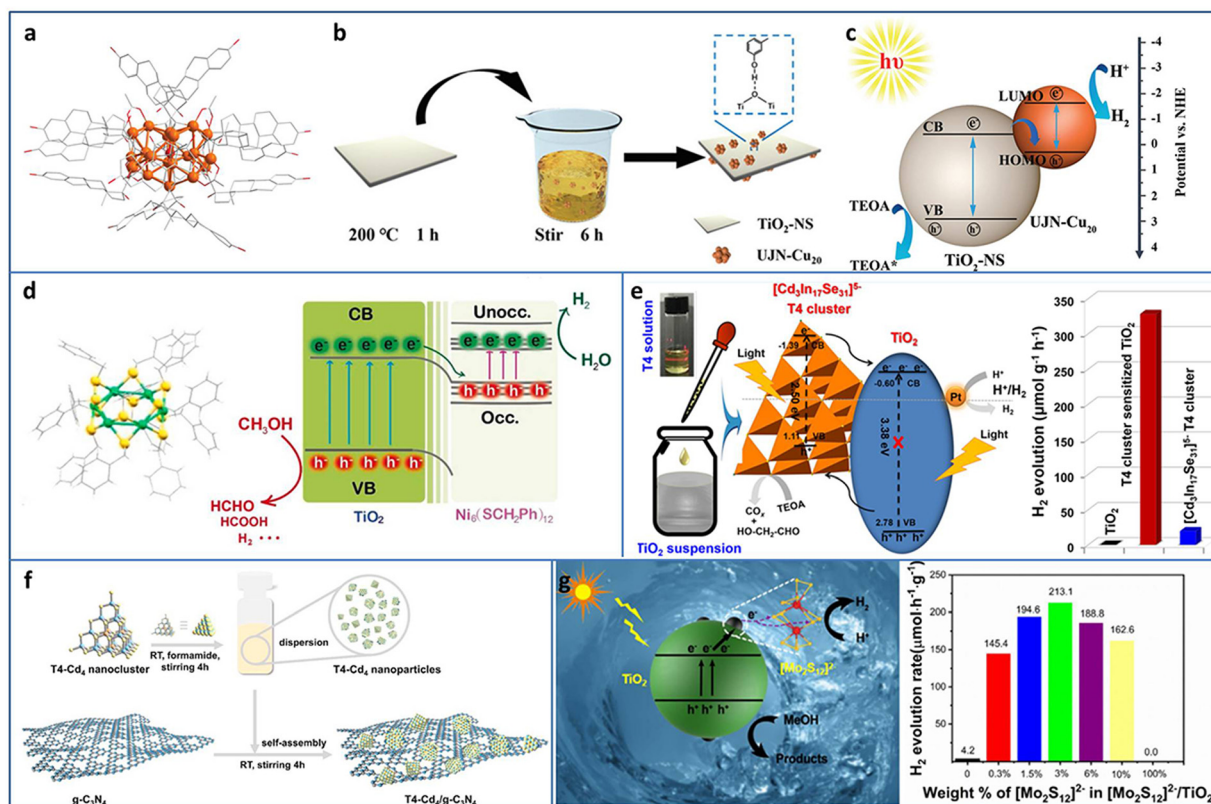


Fig. 4 (a) The crystal structure of UJN-Cu₂₀. (b) and (c) Synthesis and photocatalytic H₂ evolution mechanism of UJN-Cu₂₀@TiO₂. (d) The crystal structure of Ni₆ and the photocatalytic charge transfer of Ni₆ and TiO₂. (e) [Cd₃In₁₇Se₃₁]⁵⁻ T₄ NCs/TiO₂ for photocatalytic H₂ production. (f) Synthesis of T₄-Cd₄/g-C₃N₄. (g) [Mo₂S₁₂]²⁻ NCs and TiO₂ composites for photocatalytic H₂ production. Reproduced with permission from ref. 46–50; copyright the Royal Society of Chemistry, Elsevier B.V., and American Chemical Society.

displayed ~51 times enhancement in the photocatalytic H₂ production rate compared with TiO₂ (Fig. 4(g)).

At present, metal NCs have made encouraging progress in photocatalytic hydrogen evolution reaction. However, in most cases, hole sacrificial agents are added to consume oxidizing holes produced at the valence bands, which reduces the recombination of electron-hole pairs and effectively utilizes photogenerated electrons to obtain high hydrogen-producing activity. This operation is actually only a half reaction of photocatalytic water splitting. Although the hydrogen production activity can be improved, it will cause an increase in the actual reaction cost and additional environmental pollution. The highest pursuit of photocatalytic reaction is to achieve photocatalytic overall water splitting without sacrificial agents, and photogenerated electrons and holes can be used to produce hydrogen and oxygen with stoichiometric ratios, which is the future trend of photocatalytic development.

2.2 Photocatalytic CO₂ reduction

The excessive emission of CO₂ has caused serious environmental problems. The capture of CO₂ has been researched for decades and led to some inspiring achievements. However, the effective utilization of CO₂ is the ultimate goal of solving CO₂ emission. Several works have focused on CO₂ hydrogenation at high temperature and pressure without the

consideration of hydrogen cost. Electrocatalytic CO₂ reduction is a potential alternative strategy, but the required additional electricity is essentially another form of energy. As a green and facile method, photocatalytic CO₂ reduction to valuable C-containing products has attracted great interests benefiting from the inexhaustible solar energy.^{51–54} The first two steps of photocatalytic CO₂ reduction are the same as that of photocatalytic water splitting, except for the final step, due to the complex proton-coupled electron transfer processes and various C-containing products (*i.e.*, 2 e⁻ for CO and HCOOH, 6 e⁻ for CH₃OH, 8 e⁻ for CH₄ and CH₃COOH, 12 e⁻ for C₂H₅OH and C₂H₄, 14 e⁻ for C₂H₆) during CO₂ reduction. In addition, the energy position of CB of the photocatalyst required in theory is changed according to the targeted reduction product, as summarized by previous reported reviews.^{55,56}

Due to the accurate controllable composition and structure, atomically precise Au NCs exhibit size or structure-related light response, which makes them light harvesters in photocatalysis. However, the lack of catalytically active sites for CO₂ reduction inhibits Au NCs applications in photocatalytic CO₂ conversion. Cui *et al.* modified Au-GSH NCs with L-cys ligands to graft transition metal cations (Fe²⁺, Co²⁺, Ni²⁺, and Cu²⁺) (Fig. 5(a)).⁵⁷ The Au NCs and connected metal ions acted as light-harvesting centers and catalytic centers for photocatalytic CO₂ reduction, respectively. The photogenerated electrons transferred from the

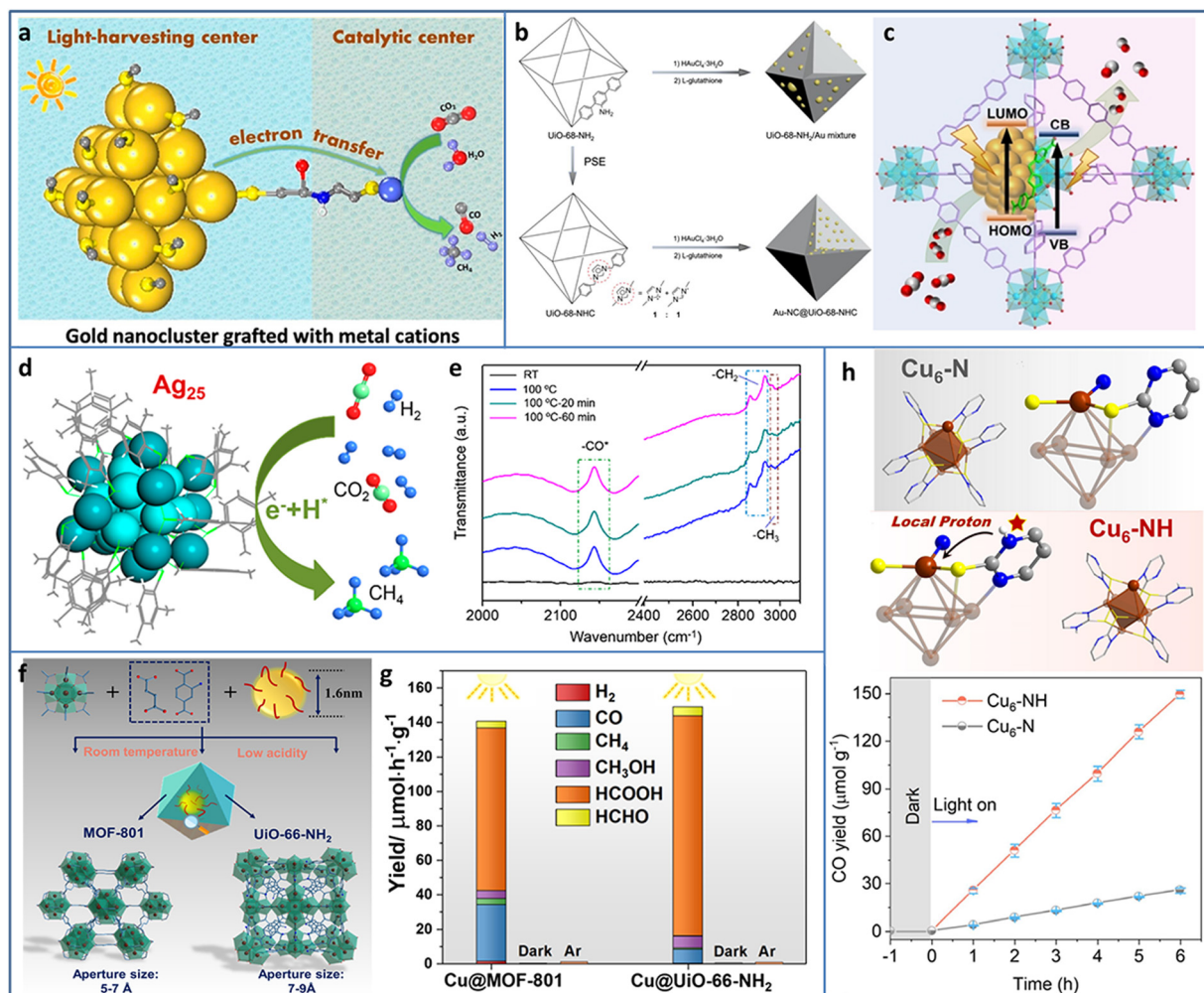


Fig. 5 (a) Au NCs grafted with transition metal cations for photocatalytic CO₂ reduction. (b) and (c) Synthesis and photocatalytic CO₂ reduction mechanism of Au-NC@UiO-68-NH₂. (d) Photoreduction of CO₂ to CH₄ and (e) time-resolved *operando* IR spectra of Ag₂₅ NCs. (f) and (g) Synthesis and photocatalytic CO₂ reduction of Cu NCs@MOFs. (h) The comparison of structure and photocatalytic CO₂ reduction activity of Cu₆-N and Cu₆-NH. Reproduced with permission from ref. 57–61; copyright American Chemical Society and Wiley-VCH GmbH.

Au NCs to the metal ions through the metal-S bridge to participate in CO₂ reduction. The metal ions type greatly influenced the photoinduced electron transfer efficiency, the donation ability of the electrons to the reactants, and the adsorption ability of the reactants, and thus led to different CO₂ conversion activities and product selectivities. The Au NCs-Co²⁺ exhibited a production rate of 3.54 μmol g_{cat}⁻¹ h⁻¹ and a selectivity of 65.2% in the photoreduction of CO₂ to CO under λ > 420 nm light irradiation in water system with TEOA as the sacrificial agent.

Most of the previously synthesized Au NCs were protected by thiol ligands due to the stable Au-S bonds. Recently, N-heterocyclic carbenes (NHCs) were used in preparing Au NCs owing to the strong Au-carbene covalent bond. In addition, NHC ligands possessed the ability of CO₂ activation, presenting reactivity in CO₂ conversion. The wide diversity in the structure of NHC ligands offered the possibility to modify the Au NCs and expand their applications. Jiang *et al.* encapsulated Au NCs in UiO-68-NHC by the NHC-assisted nucleation

method (Fig. 5(b)).⁵⁸ The Au NCs were uniformly dispersed in UiO-68-NHC with a tunable size in the range of 1.3–1.8 nm. Due to the Au-carbene covalent bond at the interface of the heterostructure, Au-NC@UiO-68-NHC showed significantly enhanced photostability. In contrast, the Au species on the amine or imidazolium-functionalized MOF showed typical aggregation. In photocatalytic CO₂ reduction, Au-NC@UiO-68-NHC showed a high CO production rate of 57.6 μmol g⁻¹ h⁻¹ under 300 W xenon lamp irradiation with 300 nm ≤ λ ≤ 800 nm in the mixture of CH₃CN and CH₃OH system (Fig. 5(c)), four times higher than that of the UiO-68-NH₂/Au mixture.

Methane is a widely used fuel and chemical raw material with high value; however, photocatalytic CO₂ reduction to CH₄ is relatively difficult due to the involvement of the eight-electron transfer process. Xiong *et al.* utilized atomically precise Ag₂₅ NCs, realizing nearly 100% selectivity in the photoreduction of CO₂ to CH₄ (Fig. 5(d)).⁵⁹ Time-resolved *operando* IR spectroscopy was used to investigate the intermediates generated during CO₂ reduction. The bands at 2142, 2854,

and 2963 cm^{-1} were assigned to $^*\text{CO}$, $-\text{CH}_2$, and $-\text{CH}_3$, respectively (Fig. 5(e)). CH_4 was formed through an $-\text{H}$ -assisted multi-electron reaction pathway. In addition, the adsorption of CO_2 on Ag_{25} NCs was energetically favorable, as confirmed by DFT calculation.

Cu NCs are considered as one of the most promising catalysts for CO_2 conversion not only due to their relatively low cost but also because of the specific ability to generate multiple carbon products. Encapsulating metal NCs in the cavity of MOFs can avoid the aggregation of NCs but trigger some new problems, such as the hindered diffusion of the reactant and uncertain distribution of active sites. Dai *et al.* proposed a facile seed-mediated growth method to synthesize gram-scale core-shell Cu NCs@MOFs at room temperature in aqueous solution (Fig. 5(f)).⁶⁰ Two benchmark Zr-based MOFs (MOF-801 and UIO-66- NH_2) were selected as the templates. Compared to the Cu NCs/MOF (Cu NCs on the surface or in the pore of MOFs), the core-shell Cu NCs@MOFs showed three times higher catalytic activity. In addition, the polar functional group of MOF played an important role in tuning the catalytic activity and selectivity. Compared to the $94 \mu\text{mol h}^{-1} \text{g}^{-1}$ photocatalytic CO_2 reduction rate of Cu NCs@MOF-801 (under 385 nm light irradiation with TEOA as the sacrificial agent), Cu NCs@UIO-66- NH_2 exhibited a 36% higher catalytic rate (Fig. 5(g)). The HCOOH product selectivity of Cu NCs@UIO-66- NH_2 was also higher than that of Cu NCs@MOF-801. X-ray absorption near edge structure/extended X-ray absorption fine structure (XANES/EXAFS) and *in situ* IR spectroscopy measurements were conducted to explore the catalytic mechanism and revealed that the Cu^+ sites at the interface between Cu NCs and MOFs were the active sites for the photoreduction of CO_2 .

Constructing stable Cu NCs with suitable band structure and active catalytic sites for photocatalytic CO_2 reduction remains a challenge. 2-Mercaptopyrimidine (PymSH) with thiol and thione tautomeric forms presents high affinity for multiple types of metal centers and is widely used as a protective ligand to stabilize NCs. In addition, the uncoordinated N atom can serve as a proton relay station, offering a local proton source for accelerating the reaction dynamics. Dong *et al.* synthesized a novel $\text{Cu}_6\text{-NH}$ NC containing local protonated N-H with high stability and semiconductor property.⁶¹ Under $\lambda > 400 \text{ nm}$ visible light irradiation, with H_2O as an electron donor, $\text{Cu}_6\text{-NH}$ showed $\sim 100\%$ selectivity for the photoreduction of CO_2 to CO (Fig. 5(h)). The other isostructural $\text{Cu}_6\text{-N}$ NCs were further synthesized to systematically investigate the ligand effect on the catalytic activity. The underlying reason of the high activity of $\text{Cu}_6\text{-NH}$ was attributed to the protonated pyrimidine N, which provided a local proton to reduce the energy barrier for the formation of the key $^*\text{COOH}$ intermediate, as demonstrated by *in situ* diffuse reflectance infrared Fourier transform spectroscopy (DRIFTS) measurements and DFT calculations.

In photocatalytic CO_2 reduction reaction, noble metal NCs, such as Au and Ag NCs, have been studied more, mainly due to the relatively mature synthesis methods and the intrinsically better stability than that of non-noble metal NCs. However, the types of products for CO_2 reduction using noble metal NCs as

catalysts are relatively simple. For example, for Au NCs, the common CO_2 reduction product is CO. In order to deeply reduce CO_2 into more valuable chemicals, more types of metal NCs need to be explored. In addition, in the current studies, only a few works have reported using water as a proton source. To achieve cleaner and greener energy conversion in the future, it is necessary to explore CO_2 reduction reaction in pure water systems. At the same time, how to efficiently transform the low concentration of CO_2 in the atmospheric environment is also a meaningful topic worth exploring.

2.3 Photocatalytic organic transformation

Utilizing solar energy, catalytic pollutant degradation and organic transformations are ideal potential solutions for green chemistry.^{62–65} Metal NCs with molecular-like discrete energy band can serve as light-harvesting antenna. In addition, the unique atom packing mode, quantum size effect, and abundant surface active sites make them potential effective catalysts for multiple types of photoredox reactions.

Atomically precise metal NCs can achieve the elaborate tuning of the catalytic performance due to the accurate and controllable size, composition, and structure. Among the various tunable strategies, metal doping is of significance for obtaining advanced catalytic activity. Cheng *et al.* synthesized serial $\text{Ag}_4\text{M}_2(\text{SPhMe}_2)_8$ ($\text{M} = \text{Ni}, \text{Pd}, \text{Pt}$) NCs ($\text{SPhMe}_2 = 2,4$ -dimethylbenzenethiol) with the same spatial geometric structure (Fig. 6(a)).⁶⁶ The overall structure is similar to a distorted hexahedron, in which four Ag atoms were at the midpoints of the four side edges and two foreign metal atoms were at the center of the top and bottom planes. Ag and M atoms formed an electron donor-acceptor pair, which was important for photocatalysis. In the photocatalytic degradation of methyl orange, $\text{Ag}_4\text{Pd}_2/\text{TiO}_2$ showed the best catalytic activity with $\sim 100\%$ degradation in 18 minutes, followed by Ag_4Pt_2 (42 minutes) and Ag_4Ni_2 (54 minutes). However, in the photocatalytic degradation of rhodamine B, the order of catalytic activity was reversed, *i.e.*, $\text{Ag}_4\text{Ni}_2 > \text{Ag}_4\text{Pt}_2 > \text{Ag}_4\text{Pd}_2$. The total difference in the catalytic performance of the three NCs in the degradation of methyl orange and rhodamine B was attributed to the alignment of the molecular orbitals near the HOMO-LUMO gap caused by different inter-molecular recombination mechanisms (complexation-induced recombination for methyl orange and collision-induced recombination for rhodamine B) (Fig. 6(b)).

Rapid charge recombination and poor stability limit the photocatalytic application of metal NCs. Building a heterostructure with cascade charge transport pathway can effectively solve the dilemma. Xiao *et al.* designed two kinds of transition TMC-metal NC-based heterostructure (CdS@PAH@Ag_9 NCs and CdSe-Au_x NCs-graphene, PAH = poly(allylamine hydrochloride)) *via* step-by-step surface modification and electrostatic self-assembly. In the CdS@PAH@Ag_9 NCs system, PAH played the dual roles of a surface charge modifier to connect $\text{Ag}_9(\text{GSH})_6$ NCs and CdS and an interfacial charge transport mediator to accelerate charge separation. Under light irradiation, the photoinduced electrons generated on the Ag_9 NCs

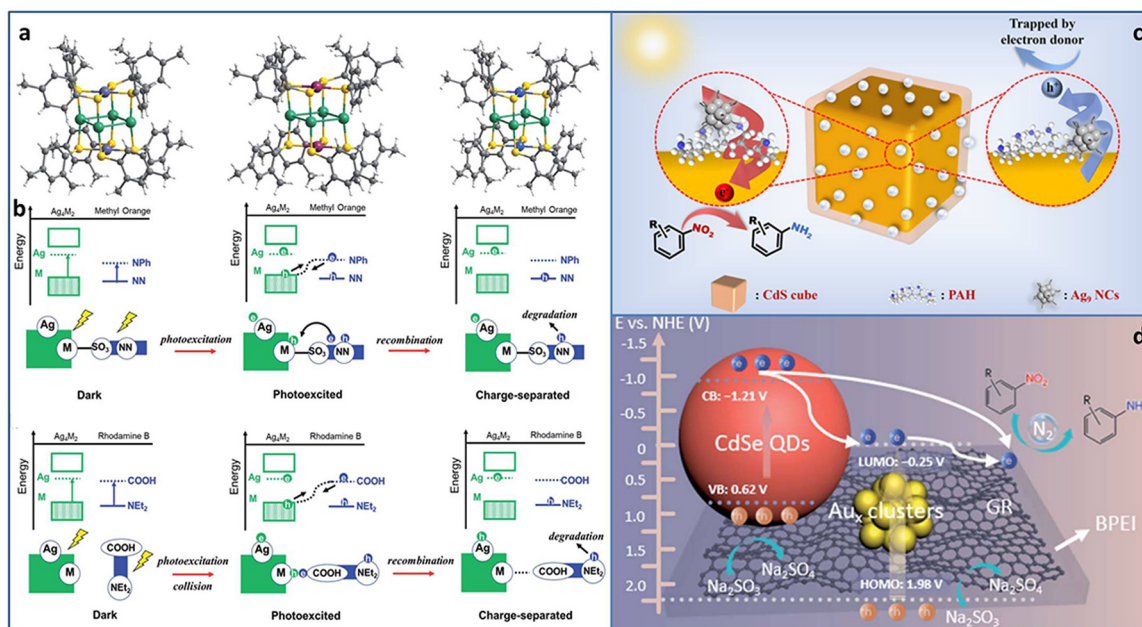


Fig. 6 (a) The crystal structure of $\text{Ag}_4\text{M}_2(\text{SPhMe}_2)_8$ ($\text{M} = \text{Ni, Pd, and Pt}$) NCs. (b) The photocatalytic mechanisms of methyl orange and rhodamine B degradation over $\text{Ag}_4\text{M}_2(\text{SPhMe}_2)_8$ ($\text{M} = \text{Ni, Pd, and Pt}$) NCs. Photocatalytic reduction of nitroaromatics to amino derivatives over (c) $\text{CdS}@PAH@Ag_9$ NCs and (d) $\text{CdSe}-\text{Au}_x$ NCs-graphene. Reproduced with permission from ref. 66–68 copyright the Royal Society of Chemistry and the American Chemical Society.

flowed to CdS with the aid of PAH; thereby the charge lifetime was effectively prolonged, leading to an enhancement in the catalytic activity for the selective anaerobic photocatalytic reduction of nitroaromatics to amino derivatives (Fig. 6(c)).⁶⁷ In the $\text{CdSe}-\text{Au}_x$ NCs-graphene system, Au_x NCs and CdSe both acted as the photosensitizer. More importantly, Au NCs were used as an intermediate charge relay mediator, and graphene provided the electron-withdrawing capability, synergistically promoting interfacial charge transfer and separation, leading to enhanced photoactivity towards the selective reduction of aromatic nitro compounds to amino derivatives (Fig. 6(d)).⁶⁸

COF is one of the most attractive porous supports due to its highly ordered structure and ultrasmall pores, offering an opportunity to uniformly load metal NCs. Deng *et al.* synthesized a two-dimensional (2D) COF with thiol chains, in which the $-\text{SH}$ groups acted as the nucleation sites for the *in situ* growth of Au NCs in COF (Fig. 7(a)).⁶⁹ Due to the strong Au-S binding force and ultrasmall pores of COF, the obtained Au NCs with uniform size were highly dispersed in the pores of the COF. Based on the formation of Au-S-COF bonding, a Z-scheme photocatalytic heterostructure was constructed for improved charge separation and photocatalytic activity. In a continuous flowing pollution system, the filter paper made by Au NCs@COF catalysts was applied in the degradation of rhodamine B and bisphenol A and showed satisfactory activity in five consecutive cycles (Fig. 7(b)).

Under light irradiation, the organic protective ligands on the surface of metal NCs may deplete by photogenerated holes, causing the coalescence or growth of NCs. Bismuth oxyhalides BiOX ($\text{X} = \text{Cl, Br, I}$), as new layer materials, are widely applied in

the photocatalytic field due to their semiconductor features. As a typical example, BiOCl consists of $[\text{Bi}_2\text{O}_2]^{2+}$ layers interleaved with two layers of Cl ions and exhibits a self-built internal electric field for improving the carrier separation. In addition, the layer structure can shorten the distance of carrier transportation from inside to the surface. Chen *et al.* fabricated $\text{Au}_{25}(\text{PPh}_3)_{10}(\text{SC}_3\text{H}_6\text{Si}(\text{OC}_2\text{H}_5)_3)_5\text{Cl}_2$ (PPh_3 = triphenylphosphine, $\text{SC}_3\text{H}_6\text{Si}(\text{OC}_2\text{H}_5)_3$ = mercaptopropyltriethoxysilane) NCs/ BiOCl heterostructure *via* the wet-impregnation method (Fig. 7(c)).⁷⁰ The 0D/2D heterostructure possessed a large amount of junctions, benefiting the effective charge transfer and separation. Besides this, the heterostructure was conducive to the stabilization of the Au NCs, preventing them from self-oxidation. Based on the analysis of the energy band structure and a series of photoelectrochemical measurements, a Z-scheme charge transfer pathway was confirmed in the Au_{25} NCs/ BiOCl heterostructure (Fig. 7(d)). The Au_{25} NCs/ BiOCl realized the photocatalytic oxidative coupling of various amine substrates and showed a high TOF of 1916 h^{-1} for benzylamine (under 100 W LED lamp irradiation in a mixture of ethanol and water system), which were 4.7 and 12773.3 times higher than that of Au_{25} NCs and 2D- BiOCl , respectively.

Currently, most photocatalytic reactions proceed under the irradiation of UV/visible light. However, nearly half of the solar spectrum is made up of the much lower energy infrared light. From the energy-saving perspective, the less energy to excite the electron transition is more attractive to researchers.⁷¹ Therefore, developing photocatalyst with near-infrared (NIR) light response is highly desired. Due to the precisely adjustable number, the type and arrangement of metal atoms, metal

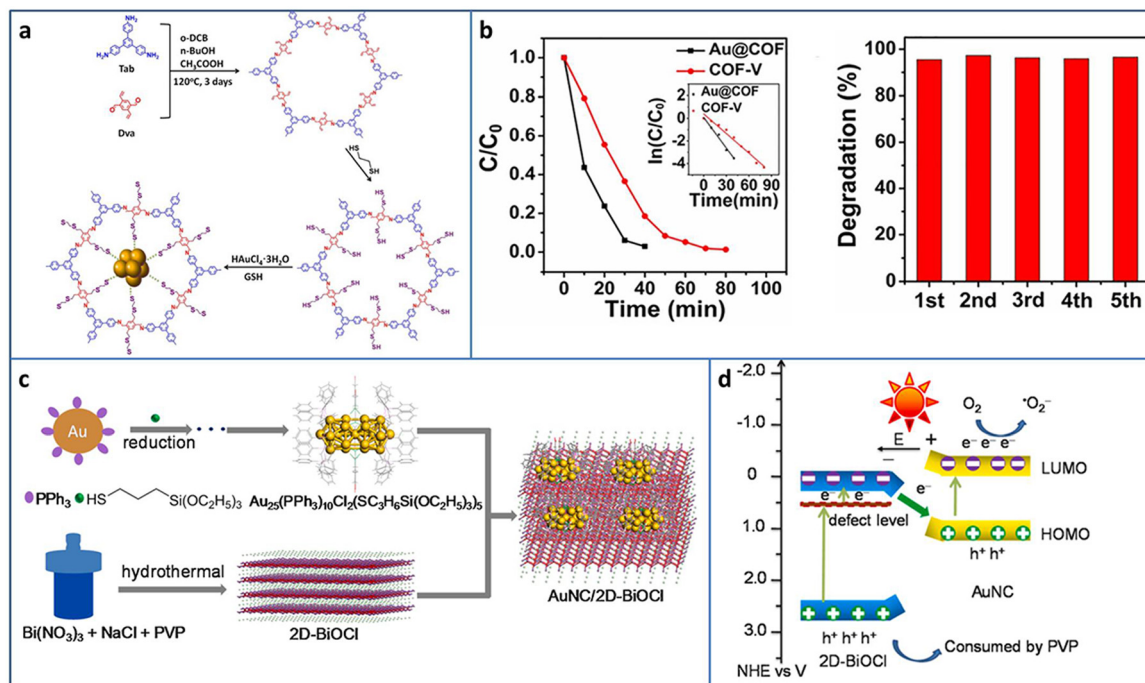


Fig. 7 (a) Synthesis of Au@COF. (b) Activity and recycling ability of the degradation of RhB Au@COF. (c) and (d) Synthesis and photocatalytic charge transfer pathway of Au₂₅ NCs/BiOCl. Reproduced with permission from ref. 69,70, copyright Wiley-VCH Verlag GmbH & Co. KGaA, Weinheim and Elsevier B.V.

NCs exhibit tunable HOMO–LUMO gap, realizing the wide light spectrum utilization from UV to NIR. Wang *et al.* synthesized Au₂₅(F-Ph)₁₈[−] (F-Ph = 3,4-difluorothiophenol) NCs *via* surface modification on the Au₂₅(PET)₁₈[−] template (Fig. 8(a)).⁷² Due to the π – π stacking between the F-Ph ligands, the modified Au₂₅(F-Ph)₁₈[−] shows improved stability compared to Au₂₅(PET)₁₈[−], reflecting the almost unchanged UV-vis characteristic peaks of Au₂₅(F-Ph)₁₈[−] in the presence of H₂O₂ and the remaining negatively charged state after irradiation. In addition, Au₂₅(F-Ph)₁₈[−] displays higher ¹O₂ production ability, indicating the enhanced catalytic activity than that of Au₂₅(PET)₁₈[−]. On the basis of these findings, Au₂₅(F-Ph)₁₈[−] NCs are used to realize the C–H functionalization of 2-aryl-1,2,3,4-tetrahydroisoquinolines (Fig. 8(b)). Under NIR light irradiation, [Au₂₅][−] is photo-excited to [Au₂₅]^{−*}, and then [Au₂₅]^{−*} transfers the energy for the formation of ¹O₂ from ³O₂ for the subsequent C–H functionalization process. From the time-dependent synthesis yield curve, it can be seen that when using 850 nm NIR LED instead the 460 nm blue LED light source, the yield of the product is significantly improved from 69% in 48 h to 99% in 8 h (Fig. 8(c)). Due to the high activity of Au₂₅(F-Ph)₁₈[−] NCs for NIR photocatalytic oxidation, it is further extended to other useful oxidation reactions, *i.e.* the selective oxidation of sulfides to sulfoxides and aerobic oxidation of β -ketoesters (Fig. 8(d) and (e)), achieving excellent catalytic performance in oxidative functionalization.

In photocatalytic organic transformation, since most of the cases are for dye degradation, the transformation of nitroaromatics to amino derivatives model reactions, it is necessary to apply NCs to more practical reactions. In the case of organic

reactants, whether NC ligands will participate in the reaction and what effect it has on the reaction activity is an attractive orientation. In addition, NCs themselves have the property of generating singlet oxygen by light excitation; thus, how to apply this property to the photocatalytic reaction is also a problem worth thinking about.

2.4 Photoelectrocatalytic reaction

Photoelectrocatalysis is a combination of photocatalysis and electrocatalysis, which can maximize the advantages of both the technologies. Compared with photocatalysis, photoelectrode can generate photogenerated electrons by sunlight irradiation, and the photogenerated charge can be separated applying a certain bias voltage to the photoelectrode, which improves the reaction activity and catalytic efficiency. Compared with electrocatalysis, the photoelectrocatalytic reaction greatly reduces the injection of external energy and can effectively reduce the energy consumption and environmental pollution. In addition, the catalyst that is not suitable for photocatalysis due to the mismatch of the energy band structure can be applied to photoelectrocatalysis under appropriate applied voltage conditions.^{73–75}

Atomically precise metal NCs can be used as photosensitizers in photoelectrochemical (PEC) cells. Wang *et al.* fabricated phenylacetylene (PA)-modified TiO₂ nanotube array (TNA) and deposited Au₂₄Ag₂₀(PhCC)₂₀(SPy)₄Cl₂ NCs (Py = pyridine) (PhCC = Phenylacetylene) based on the π – π interactions between the phenyl rings of NCs and that of the organic coating of TiO₂ (Fig. 9(a)).⁷⁶ The introduction of Au₂₄Ag₂₀ NCs enhanced the light harvesting due to its high molar extinction coefficient.

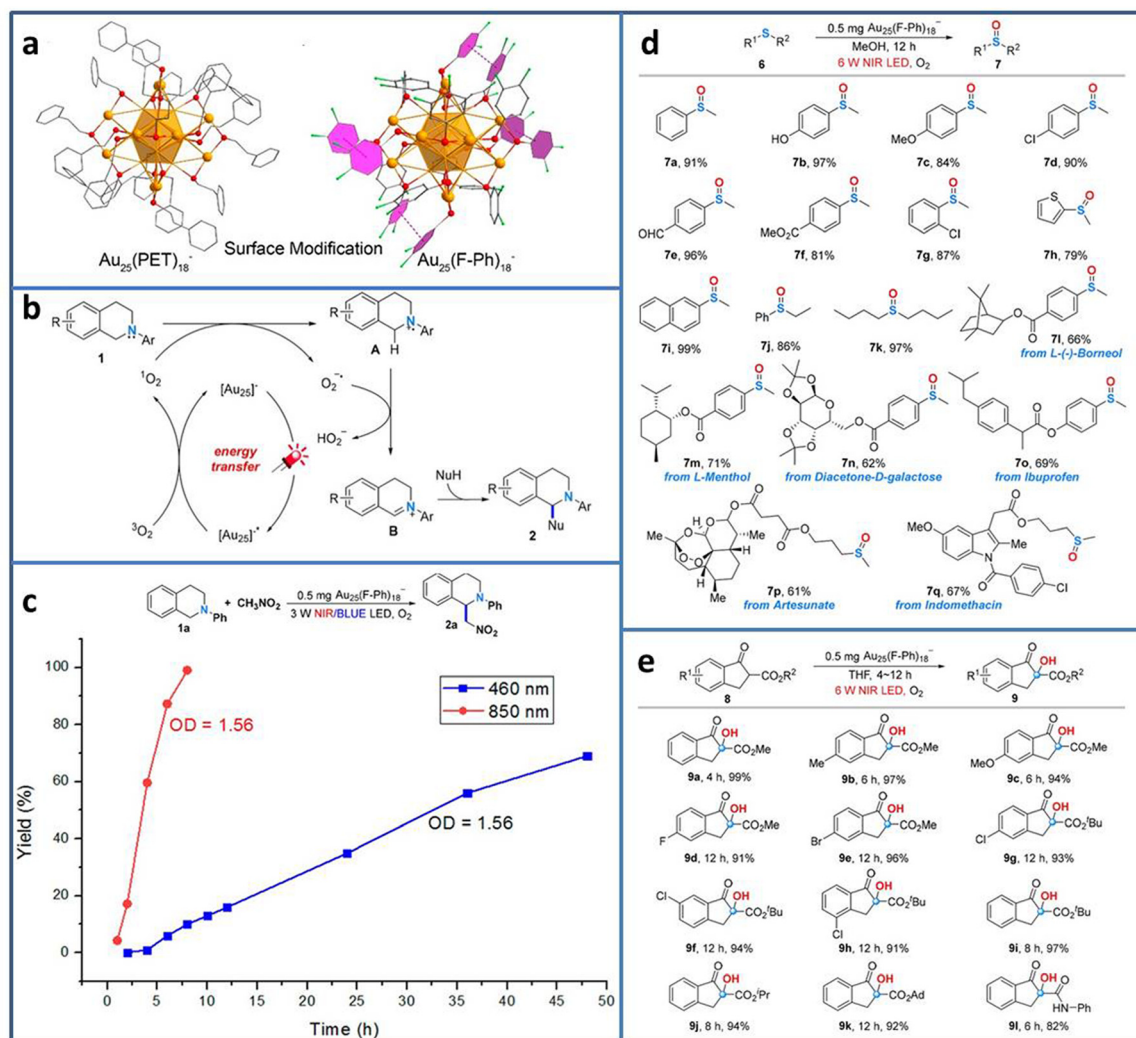


Fig. 8 (a) Structure of $\text{Au}_{25}(\text{F-Ph})_{18}^-$ and $\text{Au}_{25}(\text{PET})_{18}^-$. (b) C-H functionalization of 2-aryl-1,2,3,4-tetrahydroisoquinolines catalyzed by $\text{Au}_{25}(\text{F-Ph})_{18}^-$. (c) Time-dependent synthesis yield using $\text{Au}_{25}(\text{F-Ph})_{18}^-$ under NIR and blue LED light irradiation. (d) Oxidation of sulfides to sulfoxides and (e) aerobic oxidation of β -ketoesters using $\text{Au}_{25}(\text{F-Ph})_{18}^-$ under NIR light irradiation. Reproduced with permission from ref. 72, copyright American Chemical Society.

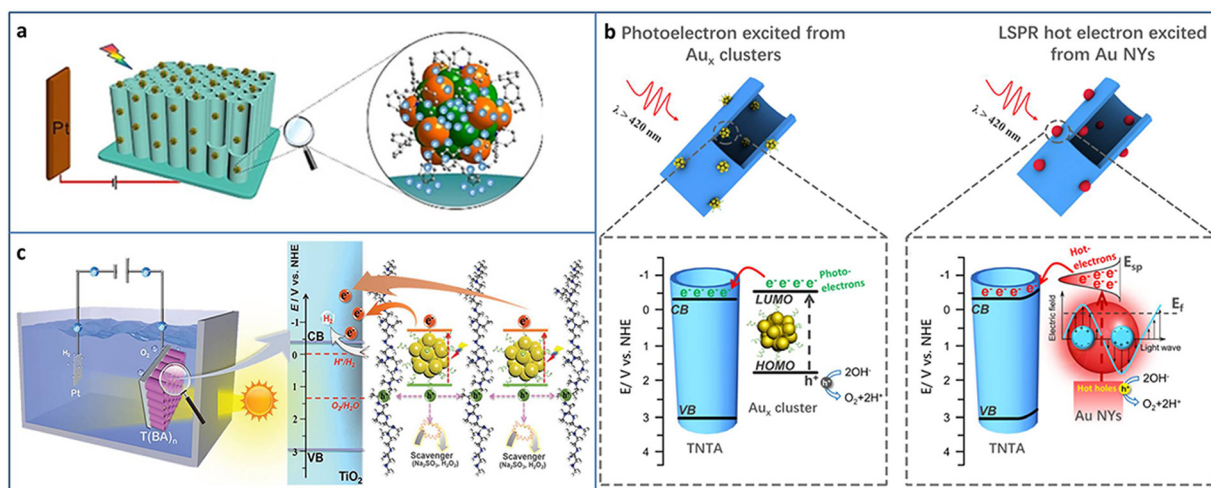


Fig. 9 (a) Synthesis of $\text{Au}_{24}\text{Ag}_{20}$ -TNA for PEC application. (b) The comparison of PEC water splitting by metal NCs and NPs. (c) PEC water splitting of the Au_x NCs-BPEI-metal oxide system. Reproduced with permission from ref. 35, 76, 77; copyright Wiley-VCH Verlag GmbH & Co. KGaA, Weinheim, and American Chemical Society.

The photocurrent of $\text{Au}_{24}\text{Ag}_{20}$ -TNA is higher than that of Au_{25} -TNA because of the higher light absorption ability and charge-separation efficiency of $\text{Au}_{24}\text{Ag}_{20}$ NCs. In addition, $\text{Au}_{24}\text{Ag}_{20}$ -TNA shows much better photostability in both neutral and basic conditions compared to Au_{25} -TNA.

It is well-known that there are great differences between atomically precise metal NCs and conventional metal NPs, such as physicochemical properties, quantum confinement effect, and photosensitization effect, especially, the electrons photoexcited from the metal NCs and the hot electrons from the surface plasmonic resonance (SPR) effect of metal NPs. Xiao *et al.* compared the performance of photoelectrochemical water splitting between metal NCs and NPs by strict control experiments (Fig. 9(b)).³⁵ TNA- Au_x NCs were fabricated by assembling Au_x @GSH NCs on TNA based on electrostatic interaction. The corresponding TNA-Au NPs were obtained by the calcination of TNA- Au_x NCs. A series of experiments such as LSV curves, applied bias photon-to-current efficiency, photocurrent response, electron impedance spectroscopy, Mott-Schottky plots and the charge carrier density calculation, open circuit voltage and the electron lifetime calculation, and incident-photon-to-current conversion efficiency was conducted to investigate the difference between the metal NCs and metal NPs-triggered charge transfer characteristics. In terms of interfacial charge separation and transfer, the photoelectrons from Au_x @GSH NCs are superior to the hot electrons from plasmonic Au NPs. The PEC water splitting mechanisms of TNA- Au_x NCs and TNA-Au NPs were further revealed. Au_x @GSH NCs with HOMO-LUMO gap are able to serve as a small-band-gap semiconductor and can be photoexcited to generate electrons and holes. Due to the band alignment, the electrons in the LUMO of Au_x NCs can transfer to the CB of TiO_2 and then flow to the photocathode to produce hydrogen and generate photocurrent. Au NPs are able to be photoexcited due to the SPR effect and generate hot electrons. The hot electrons are injected into the CB of TiO_2 by surpassing the Schottky barrier. The holes oxidize water to oxygen at the photoanode.

To improve the stability and carrier utilization efficiency of NCs-based photosystems, Xiao *et al.* constructed an NCs-based multilayer heterostructure with spatially separated charge transport pathways *via* the layer-by-layer assembly strategy. GSH-protected Au_x NCs and branched poly-ethylenimine (BPEI) have opposite surface charge state, and they are alternately deposited on the metal oxide (*i.e.*, TiO_2 , WO_3 , and Fe_2O_3). Au_x NCs serve as lightharvesting antennas and generate photocarriers. BPEI interim layer contributes to the tandem hole transport. As a result, the charge transfer cascade is motivated, leading to enhanced PEC water splitting activity (Fig. 9(c)).⁷⁷

When the particle size becomes extremely small, the space charge layer cannot be formed, which affects the carrier separation ability. However, in the PEC system, even if the very small particles do not form a space charge layer, the photogenerated charge carriers can also be driven by the applied potential from the photoelectrode material to the opposite electrode so as to achieve effective separation. There is no doubt that the photoelectrode catalyst is the most important component, which

determines the reaction process and the catalytic efficiency of the PEC system. Metal NCs can act as catalysts, photosensitizers, charge transport media and other roles in the PEC process, but the NCs are small in size and easy to aggregate, requiring a suitable matrix as the support and stabilizer. In addition, the PEC process is also affected by various other factors, such as solution conductivity and pH, applied bias voltage, light intensity, and temperature. The PEC process is more complex than the photocatalytic process; thus, it is still very challenging to clearly identify the role of NCs in it and figure out the factors affecting its efficiency.

2.5 Other photocatalytic reaction

Photocatalytic reduction of N_2 to NH_3 . NH_3 is an important chemical and energy carrier. At present, the traditional Haber-Bosch process of industrial NH_3 synthesis is facing more and more severe challenges, such as high energy consumption, high cost and harmful gas emission. The photocatalytic reduction of N_2 to NH_3 has attracted extensive attention and research interests because of its similar advantages to biological N_2 fixation, such as simple reaction system, mild reaction conditions, environmental friendliness, low cost, safety, and ease of performance regulation and has shown great potential in the field of NH_3 synthesis.^{78–80} Unlike the conventional Haber-Bosch method, the synthesis of NH_3 by photocatalytic N_2 reduction does not require the use of H_2 , that is, H_2O provides the proton. Ammonia can be directly synthesized from water and nitrogen under ambient conditions using sunlight as an energy source ($\text{N}_2 + 3\text{H}_2\text{O} = 2\text{NH}_3 + 1.5\text{O}_2$).⁸¹

Metal NCs with excitonic behavior are capable of generating electrons induced by solar energy and donating electrons to N_2 for its reduction. Sun *et al.* utilized TiO_2 with oxygen vacancy ($\text{TiO}_2\text{-V}_\text{o}$) to support $\text{Au}_4\text{Ru}_2(\text{PPh}_3)_2(\text{SC}_2\text{H}_4\text{Ph})_8$ NCs.⁸² Under light irradiation, the excited Au_4Ru_2 NCs generated photoinduced electron-hole pairs. The photogenerated carriers effectively separated between Au_4Ru_2 NCs and $\text{TiO}_2\text{-V}_\text{o}$, in which the electrons transferred to the Ru atoms and then injected to N_2 for its activation. $\text{TiO}_2\text{-V}_\text{o}$ was responsible for the water splitting to provide the proton for N_2 hydrogenation (Fig. 10(a)). In comparison with a series of homometal Au_n NCs ($n = 8, 9, 11, 18, 23, 24, 25, 28, 36, 44$), the alloyed Au_4Ru_2 NCs can effectively activate N_2 . The distance between N_2 and NCs in the Au_n NCs was larger than 3.2 Å, indicating the physical adsorption of N_2 on these Au_n NCs (Fig. 10(b)). On the contrary, N_2 was closer to Au_4Ru_2 NCs with a distance of 2.14 Å and 1.84 Å for the side-on and end-on configuration, respectively, suggesting the chemical adsorption of N_2 on Au_4Ru_2 NCs. Au_4Ru_2 NCs/ $\text{TiO}_2\text{-V}_\text{o}$ showed a NH_3 production rate of $44.5 \mu\text{mol g}^{-1} \text{h}^{-1}$, 3 times higher than that of Au_n NCs/ $\text{TiO}_2\text{-V}_\text{o}$.

Photocatalytic H_2O_2 production. The traditional industrial production of H_2O_2 is based on the anthraquinone process using hydrogen and oxygen. This method is a high energy consumption process, requires toxic solvents and expensive precious metal catalysts, and produces a large amount of side reaction waste. In recent years, more and more attention has been paid to the production of high value-added chemical H_2O_2

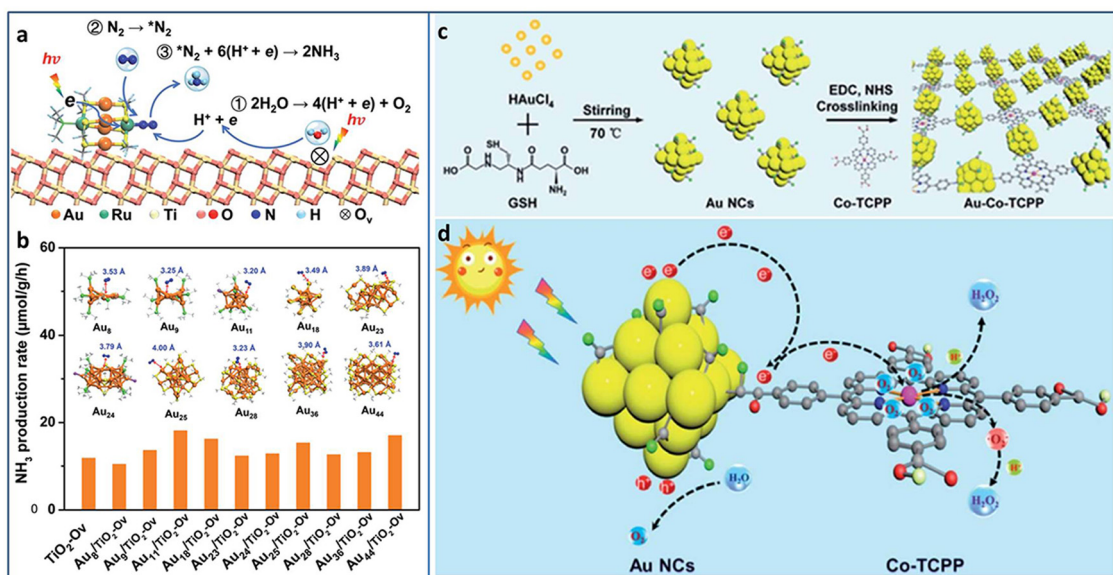


Fig. 10 (a) Photocatalytic N₂ reduction mechanism on Au₄Ru₂/TiO₂-O_v. (b) The photocatalytic N₂ reduction activity of homometal Au_n NCs ($n = 8, 9, 11, 18, 23, 24, 25, 28, 36$, and 44) on TiO₂-O_v. Inset: The structures of the Au_n NCs, and the distance between N₂ and these Au_n NCs. (c) and (d) Preparation and photocatalytic H₂O₂ production of the Au-Co-TCPP. Reproduced with permission from ref. 82 and 83, copyright the Royal Society of Chemistry.

through photocatalytic technology.^{84–87} In general, photocatalytic H₂O₂ production includes two mainstream methods, one is O₂ reduction reaction and the other one is water oxidation reaction. For O₂ reduction to generate H₂O₂, it can be classified as two situations: one is the direct pathway involving the one-step two-electron process ($O_2 + 2H^+ + 2e^- \rightarrow H_2O_2$ (+0.68 V vs. NHE)), and the other one is the two-step one-electron indirect pathway ($O_2 + e^- \rightarrow \cdot O_2^-$ (−0.33 V vs. NHE); $\cdot O_2^- + 2H^+ + e^- \rightarrow H_2O_2$ (+1.44 V vs. NHE)).^{84,88}

Xue *et al.* designed and grafted multifunctional Co porphyrin molecule on the surface of Au NCs by ligand engineering strategy to obtain three-in-one functionalized Au-Co-TCPP (Fig. 10(c)).⁸³ The Au-Co-TCPP exhibited enhanced visible light absorption, promoted charge separation efficiency, and more active sites for photocatalysis (Fig. 10(d)). Au-Co-TCPP showed an outstanding performance of 235.93 μmol in photocatalytic H₂O₂ production within 60 minutes, 2.2 times higher than that of Au NCs. By introducing the scavenger of O₂^{•−}, the H₂O₂ production mechanism showed that the two-electron O₂ reduction was the main pathway over Au-Co-TCPP. In addition, the high-spin state of Co²⁺ in Au-Co-TCPP was also beneficial to the two-electron O₂ reduction, as confirmed by the control experiment with Au-2H-TCPP.

3. Conclusions and perspectives

Due to the strong wide spectra light response and molecule-like discrete energy levels, the atomically precise metal NCs as promising photocatalysts have been widely applied in photocatalytic water-splitting, CO₂ conversion, organic transformation, N₂ fixation, H₂O₂ production, and PEC application. For catalytic reactions stimulated by light as an energy source, the

primary consideration is the effective use of light. Therefore, in order to construct an effective NCs-based photocatalyst, the premise is to expand the light absorption range, which can be achieved from the aspects of adjusting the size of the NCs, heteroatom doping, ligand engineering, *etc.* At the same time, coupling a semiconductor with a wide spectral response is also one of the feasible strategies. Secondly, photogenerated electrons and holes can effectively migrate to the surface of the photocatalyst and participate in the subsequent redox reaction rather than recombination inside the catalyst, which requires the photocatalyst to have high carrier separation efficiency. For the NCs-based photocatalytic system, the electrons and holes generated by isolated NCs are prone to recombination due to their small size, resulting in fewer carriers to take part in the reaction. Therefore, as summarized above, choosing semiconductors with appropriate energy level structures to form heterojunctions is a strategy that can effectively suppress the recombination of electrons and holes pairs, thereby improving the photocatalytic activity. In addition, this way of loading NCs on the support also reduces the possibility of NCs aggregation to a certain extent and improves the stability under light irradiation, which is very important for practical applications. Despite the above progress, there are still numerous fundamental mechanisms that need to be investigated in depth and application obstacles that need to be overcome with regard to the photocatalysis of metal NCs. From our perspective, the current challenges and future opportunities are provided below.

1. Considering that most of the sunlight is infrared light, it is necessary to develop metal NCs that are responsive to infrared light to make full use of sunlight and achieve high photocatalytic conversion efficiency. In addition, Au, Ag, Pt and other noble metal NCs have been mainly applied in

photocatalysis to date. In the long run, it is urgent to develop non-noble metal NCs with high reserves, low prices and photoactivity.

2. The property of metal NCs is dependent on various factors including size, core structure, surface motifs, and ligands. At present, several studies on the structure–activity relationships are mixed with changes in multiple parameters. Therefore, it is necessary to develop more series of atomically precise metal NCs with only a single parameter variable change so as to provide an ideal platform for finely exploring the relationship between the catalyst structure and activity.

3. Photocatalysis technology is a highly promising way of energy conversion involving all aspects. For now, the application of metal NCs in the field of photocatalysis is still limited. The feasibility of the photocatalytic reaction can be preliminarily speculated from the position of the electronic energy level of the catalyst and the redox potential of the reactant/product. Therefore, for specific target reactions, metal NCs with specific electronic structures can be synthesized by precisely regulating the size, doping, ligand and charge state, which is also of great significance for expanding the application range of metal NCs photocatalysis.

4. The poor photostability of metal NCs is a major issue in practical application. Especially, under strong light irradiation, will the ligands will fall off? How many ligands will fall off? If a ligand falls off, what is the fragment that falls off, is it the whole ligand, or some part of the ligand? What sites on the NCs are the true centers with catalytic activity? What kinds of ligands are favorable for photoinduced charge transfer? These fundamental problems require sophisticated characterization techniques for further analysis. In addition, the ligand is composed of organic molecules, which may be converted into a carbon layer outside the metal NCs, causing activity loss, and how to avoid this situation needs serious consideration.

5. Coupling with the other semiconductor to construct NCs-based heterostructures has been recently proposed as an effective strategy to improve the stability of NCs. At present, the synthesis methods of NCs-based composites mainly focus on wet impregnation, electrostatic attraction, coordination assembly, *etc.* It is necessary to develop simple, facile and general synthesis methods of NCs-based composites with intimate interface contact. In addition, the energy band alignment between the NCs and the other semiconductor needs to be paid attention to form directional charge flow. The determination of the reaction sites and the charge transfer pathway in NCs-based composite photocatalysts and the influence of the interface of the NCs-based composite on the charge transport efficiency need to be investigated in-depth.

Overall, atomically precise metal NCs have some incomparable advantages that make them potential photocatalysts. Although there are still some difficulties and challenges, a large number of studies have tried to solve these problems. It is believed that great contribution will be made in NCs photocatalysis in the near future.

Data availability

No primary research results, software or code have been included and no new data were generated or analysed as part of this review.

Conflicts of interest

The authors declare no conflicts of interests.

Acknowledgements

We acknowledge the financial support of the Natural Science Research Project of Universities in Anhui Province (KJ2021ZD0001), Natural Science Foundation of Anhui Province (2208085MB20).

References

- 1 C. Zhuang, H. Qi, X. Cheng, G. Chen, C. Gao, L. Wang, S. Sun, J. Zou and X. Han, *Angew. Chem., Int. Ed.*, 2019, **58**, 18627–18633.
- 2 Y. Du, H. Sheng, D. Astruc and M. Zhu, *Chem. Rev.*, 2020, **120**, 526–622.
- 3 L. Liu and A. Corma, *Chem. Rev.*, 2023, **123**, 4855–4933.
- 4 X. Kang, Y. Li, M. Zhu and R. Jin, *Chem. Soc. Rev.*, 2020, **49**, 6443–6514.
- 5 X. Yuan and M. Zhu, *Inorg. Chem. Front.*, 2023, **10**, 3995–4007.
- 6 C. Zhuang, W. Li, Y. Chang, S. Li, Y. Zhang, Y. Li, J. Gao, G. Chen and Z. Kang, *J. Mater. Chem. A*, 2024, **12**, 5711–5718.
- 7 M. Sayed, J. Yu, G. Liu and M. Jaroniec, *Chem. Rev.*, 2022, **122**, 10484–10537.
- 8 C. Gao, J. Low, R. Long, T. Kong, J. Zhu and Y. Xiong, *Chem. Rev.*, 2020, **120**, 12175–12216.
- 9 L. Zhang, J. Ran, S.-Z. Qiao and M. Jaroniec, *Chem. Soc. Rev.*, 2019, **48**, 5184–5206.
- 10 X. Kang and M. Zhu, *Chem. Soc. Rev.*, 2019, **48**, 2422–2457.
- 11 L. Liu and A. Corma, *Chem. Rev.*, 2018, **118**, 4981–5079.
- 12 X. Du and R. Jin, *ACS Nano*, 2019, **13**, 7383–7387.
- 13 H. Liang, Q. Chen, Q.-L. Mo, Y. Wu and F.-X. Xiao, *J. Mater. Chem. A*, 2023, **11**, 9401–9426.
- 14 T. Kawawaki, Y. Kataoka, S. Ozaki, M. Kawachi, M. Hirata and Y. Negishi, *Chem. Commun.*, 2021, **57**, 417–440.
- 15 Q.-L. Mo, B.-J. Liu and F.-X. Xiao, *J. Phys. Chem. C*, 2021, **125**, 22421–22428.
- 16 R. Qin, K. Liu, Q. Wu and N. Zheng, *Chem. Rev.*, 2020, **120**, 11810–11899.
- 17 X. Cai, G. Li, W. Hu and Y. Zhu, *ACS Catal.*, 2022, **12**, 10638–10653.
- 18 D. Yang, J. Wang, Q. Wang, Z. Yuan, Y. Dai, C. Zhou, X. Wan, Q. Zhang and Y. Yang, *ACS Nano*, 2022, **16**, 15681–15704.
- 19 H. Yan, H. Xiang, J. Liu, R. Cheng, Y. Ye, Y. Han and C. Yao, *Small*, 2022, **18**, 2200812.

- 20 D. Yang, Y. Sun, X. Cai, W. Hu, Y. Dai, Y. Zhu and Y. Yang, *CCS Chem.*, 2021, **4**, 66–94.
- 21 Q. You, H. Wang, Y. Zhao, W. Fan, W. Gu, H.-L. Jiang and Z. Wu, *J. Am. Chem. Soc.*, 2024, **146**, 9026–9035.
- 22 H. Wang, X. Liu, W. Yang, G. Mao, Z. Meng, Z. Wu and H.-L. Jiang, *J. Am. Chem. Soc.*, 2022, **144**, 22008–22017.
- 23 Y.-M. Li, J. Hu and M. Zhu, *Coord. Chem. Rev.*, 2023, **495**, 215364.
- 24 A. Dhakshinamoorthy, Z. Li, S. Yang and H. Garcia, *Chem. Soc. Rev.*, 2024, **53**, 3002–3035.
- 25 C. Bie, L. Wang and J. Yu, *Chem*, 2022, **8**, 1567–1574.
- 26 S. Nishioka, F. E. Osterloh, X. Wang, T. E. Mallouk and K. Maeda, *Nat. Rev. Methods Primers*, 2023, **3**, 42.
- 27 B.-J. Ng, L. K. Putri, X. Y. Kong, Y. W. Teh, P. Pasbakhsh and S.-P. Chai, *Adv. Sci.*, 2020, **7**, 1903171.
- 28 Y. Li, C. Zhuang, S. Qiu, J. Gao, Q. Zhou, Z. Sun, Z. Kang and X. Han, *Appl. Catal., B*, 2023, **337**, 122881.
- 29 K. Qi, C. Zhuang, M. Zhang, P. Gholami and A. Khataee, *J. Mater. Sci. Technol.*, 2022, **123**, 243–256.
- 30 Y. Negishi, M. Mizuno, M. Hirayama, M. Omatoi, T. Takayama, A. Iwase and A. Kudo, *Nanoscale*, 2013, **5**, 7188–7192.
- 31 X. Lu, A. Tong, D. Luo, F. Jiang, J. Wei, Y. Huang, Z. Jiang, Z. Lu and Y. Ni, *J. Mater. Chem. A*, 2022, **10**, 4594–4600.
- 32 X. Huang, X. Li, Q. Luan, K. Zhang, Z. Wu, B. Li, Z. Xi, W. Dong and G. Wang, *Nano Res.*, 2021, **14**, 4250–4257.
- 33 Y. Li, L. Yang, H. He, L. Sun, H. Wang, X. Fang, Y. Zhao, D. Zheng, Y. Qi, Z. Li and W. Deng, *Nat. Commun.*, 2022, **13**, 1355.
- 34 C. Wang, P. Lv, D. Xue, Y. Cai, X. Yan, L. Xu, J. Fang and Y. Yang, *ACS Sustainable Chem. Eng.*, 2018, **6**, 8447–8457.
- 35 X.-C. Dai, M.-H. Huang, Y.-B. Li, T. Li, S. Hou, Z.-Q. Wei and F.-X. Xiao, *J. Phys. Chem. C*, 2020, **124**, 4989–4998.
- 36 X.-Y. Fu, Z.-Q. Wei, S. Xu, X. Lin, S. Hou and F.-X. Xiao, *J. Phys. Chem. Lett.*, 2020, **11**, 9138–9143.
- 37 A. Yao, Y. Du, M. Han, Y. Wang, J. Hu, Q. Zhu, H. Sheng and M. Zhu, *Nano Res.*, 2023, **16**, 1527–1532.
- 38 T. Kawawaki, Y. Kataoka, M. Hirata, Y. Akinaga, R. Takahata, K. Wakamatsu, Y. Fujiki, M. Kataoka, S. Kikkawa, A. S. Alotabi, S. Hossain, D. J. Osborn, T. Teranishi, G. G. Andersson, G. F. Metha, S. Yamazoe and Y. Negishi, *Angew. Chem., Int. Ed.*, 2021, **60**, 21340–21350.
- 39 Z. Li, W. Huang, J. Liu, K. Lv and Q. Li, *ACS Catal.*, 2021, **11**, 8510–8520.
- 40 X. Yan, X.-Y. Fu and F.-X. Xiao, *Adv. Funct. Mater.*, 2023, **33**, 2303737.
- 41 H. Liang, B.-J. Liu, B. Tang, S.-C. Zhu, S. Li, X.-Z. Ge, J.-L. Li, J.-R. Zhu and F.-X. Xiao, *ACS Catal.*, 2022, **12**, 4216–4226.
- 42 Y. Wang, X.-H. Liu, Q. Wang, M. Quick, S. A. Kovalenko, Q.-Y. Chen, N. Koch and N. Pinna, *Angew. Chem., Int. Ed.*, 2020, **59**, 7748–7754.
- 43 H. Wang, X. Zhang, W. Zhang, M. Zhou and H.-L. Jiang, *Angew. Chem., Int. Ed.*, 2024, e202401443.
- 44 M. S. Bootharaju, C. W. Lee, G. Deng, H. Kim, K. Lee, S. Lee, H. Chang, S. Lee, Y.-E. Sung, J. S. Yoo, N. Zheng and T. Hyeon, *Adv. Mater.*, 2023, **35**, 2207765.
- 45 Q. Zhu, H. Shen, C. Han, L. Huang, Y. Zhou, Y. Du, X. Kang and M. Zhu, *Nano Res.*, 2024, **17**, 5002–5010.
- 46 Y.-D. Cao, H.-P. Hao, H.-S. Liu, D. Yin, M.-L. Wang, G.-G. Gao, L.-L. Fan and H. Liu, *Nanoscale*, 2021, **13**, 16182–16188.
- 47 F. Tian, J. Chen, F. Chen, Y. Liu, Y. Xu and R. Chen, *Appl. Catal., B*, 2021, **292**, 120158.
- 48 Y. Wang, J. Li, Q. Hu, M. Hao, Y. Liu, L. Gong, R. Li and X. Huang, *ACS Appl. Mater. Interfaces*, 2021, **13**, 40562–40570.
- 49 Z. Wu, X.-L. Wang, X. Wang, X. Xu, D.-S. Li and T. Wu, *Chem. Eng. J.*, 2021, **426**, 131216.
- 50 R. Zhang, K. Gong, F. Du and S. Cao, *Int. J. Hydrogen Energy*, 2022, **47**, 19570–19579.
- 51 S. Fang, M. Rahaman, J. Bharti, E. Reisner, M. Robert, G. A. Ozin and Y. H. Hu, *Nat. Rev. Methods Primers*, 2023, **3**, 62.
- 52 J. Fu, K. Jiang, X. Qiu, J. Yu and M. Liu, *Mater. Today*, 2020, **32**, 222–243.
- 53 Z. Jiang, H. Sun, T. Wang, B. Wang, W. Wei, H. Li, S. Yuan, T. An, H. Zhao, J. Yu and P. K. Wong, *Energy Environ. Sci.*, 2018, **11**, 2382–2389.
- 54 D. Li, M. Kassymova, X. Cai, S.-Q. Zang and H.-L. Jiang, *Coord. Chem. Rev.*, 2020, **412**, 213262.
- 55 K. Sun, Y. Qian and H.-L. Jiang, *Angew. Chem., Int. Ed.*, 2023, **62**, e202217565.
- 56 E. Nikoloudakis, I. López-Duarte, G. Charalambidis, K. Ladomenou, M. Ince and A. G. Coutsolelos, *Chem. Soc. Rev.*, 2022, **51**, 6965–7045.
- 57 X. Cui, J. Wang, B. Liu, S. Ling, R. Long and Y. Xiong, *J. Am. Chem. Soc.*, 2018, **140**, 16514–16520.
- 58 Y. Jiang, Y. Yu, X. Zhang, M. Weinert, X. Song, J. Ai, L. Han and H. Fei, *Angew. Chem., Int. Ed.*, 2021, **60**, 17388–17393.
- 59 Y. Xiong, H. Chen, Y. Hu, S. Yang, X. Xue, L. He, X. Liu, J. Ma and Z. Jin, *Nano Lett.*, 2021, **21**, 8693–8700.
- 60 S. Dai, T. Kajiwarra, M. Ikeda, I. Romero-Muñiz, G. Patriarche, A. E. Platero-Prats, A. Vimont, M. Daturi, A. Tissot, Q. Xu and C. Serre, *Angew. Chem., Int. Ed.*, 2022, **61**, e202211848.
- 61 J.-P. Dong, Y. Xu, X.-G. Zhang, H. Zhang, L. Yao, R. Wang and S.-Q. Zang, *Angew. Chem., Int. Ed.*, 2023, **62**, e202313648.
- 62 Y.-Z. Cheng, W. Ji, X. Wu, X. Ding, X.-F. Liu and B.-H. Han, *Appl. Catal., B*, 2022, **306**, 121110.
- 63 S. Zhang, W. Huang, X. Fu, X. Zheng, S. Meng, X. Ye and S. Chen, *Appl. Catal., B*, 2018, **233**, 1–10.
- 64 X. Wu, N. Luo, S. Xie, H. Zhang, Q. Zhang, F. Wang and Y. Wang, *Chem. Soc. Rev.*, 2020, **49**, 6198–6223.
- 65 N.-Y. Huang, Y.-T. Zheng, D. Chen, Z.-Y. Chen, C.-Z. Huang and Q. Xu, *Chem. Soc. Rev.*, 2023, **52**, 7949–8004.
- 66 X. Cheng, X. Sui, J. Xu, X. Liu, M. Chen and Y. Zhu, *RSC Adv.*, 2021, **11**, 32526–32532.
- 67 Q. Chen, X.-Z. Ge, L. Yu and F.-X. Xiao, *Inorg. Chem.*, 2023, **62**, 19358–19365.
- 68 S. Hou, M.-H. Huang and F.-X. Xiao, *J. Mater. Chem. A*, 2022, **10**, 7006–7012.
- 69 Y. Deng, Z. Zhang, P. Du, X. Ning, Y. Wang, D. Zhang, J. Liu, S. Zhang and X. Lu, *Angew. Chem., Int. Ed.*, 2020, **59**, 6082–6089.

- 70 H. Chen, L. Peng, Y. Bian, X. Shen, J. Li, H.-C. Yao, S.-Q. Zang and Z. Li, *Appl. Catal., B*, 2021, **284**, 119704.
- 71 C. Han, B. K. Kundu, Y. Liang and Y. Sun, *Adv. Mater.*, 2024, **36**, 2307759.
- 72 S. Wang, L. Tang, B. Cai, Z. Yin, Y. Li, L. Xiong, X. Kang, J. Xuan, Y. Pei and M. Zhu, *J. Am. Chem. Soc.*, 2022, **144**, 3787–3792.
- 73 T. Yao, X. An, H. Han, J. Q. Chen and C. Li, *Adv. Energy Mater.*, 2018, **8**, 1800210.
- 74 Y. Song, Y. Wu, S. Cao, Y. Zhang, D. Luo, J. Gao, Z. Li, L. Sun and J. Hou, *Adv. Energy Mater.*, 2022, **12**, 2201782.
- 75 M. Faraji, M. Yousefi, S. Yousefzadeh, M. Zirak, N. Naseri, T. H. Jeon, W. Choi and A. Z. Moshfegh, *Energy Environ. Sci.*, 2019, **12**, 59–95.
- 76 Y. Wang, X.-H. Liu, S. A. Kovalenko, Q.-Y. Chen and N. Pinna, *Chem. – Eur. J.*, 2019, **25**, 4814–4820.
- 77 Q.-L. Mo, X.-C. Dai and F.-X. Xiao, *Small*, 2023, **19**, 2302372.
- 78 Y. Zhao, L. Zheng, R. Shi, S. Zhang, X. Bian, F. Wu, X. Cao, G. I. N. Waterhouse and T. Zhang, *Adv. Energy Mater.*, 2020, **10**, 2002199.
- 79 S. Zhang, Y. Zhao, R. Shi, G. I. N. Waterhouse and T. Zhang, *EnergyChem*, 2019, **1**, 100013.
- 80 B. Sun, S. Lu, Y. Qian, X. Zhang and J. Tian, *Carbon Energy*, 2023, **5**, e305.
- 81 S. Lin, X. Zhang, L. Chen, Q. Zhang, L. Ma and J. Liu, *Green Chem.*, 2022, **24**, 9003–9026.
- 82 Y. Sun, W. Pei, M. Xie, S. Xu, S. Zhou, J. Zhao, K. Xiao and Y. Zhu, *Chem. Sci.*, 2020, **11**, 2440–2447.
- 83 Q. Xue, Z. Wang, S. Han, Y. Liu, X. Dou, Y. Li, H. Zhu and X. Yuan, *J. Mater. Chem. A*, 2022, **10**, 8371–8377.
- 84 J. Qiu, D. Dai and J. Yao, *Coord. Chem. Rev.*, 2024, **501**, 215597.
- 85 W. Fang and L. Wang, *Catalysts*, 2023, **13**, 1325.
- 86 X. Xu, Y. Sui, W. Chen, W. Huang, X. Li, Y. Li, D. Liu, S. Gao, W. Wu, C. Pan, H. Zhong, H.-R. Wen and M. Wen, *Appl. Catal., B*, 2024, **341**, 123271.
- 87 C. Zhuang, Y. Chang, W. Li, S. Li, P. Xu, H. Zhang, Y. Zhang, C. Zhang, J. Gao, G. Chen, T. Zhang, Z. Kang and X. Han, *ACS Nano*, 2024, **18**, 5206–5217.
- 88 C. Zhuang, W. Li, T. Zhang, J. Li, Y. Zhang, G. Chen, H. Li, Z. Kang, J. Zou and X. Han, *Nano Energy*, 2023, **108**, 108225.